UDC 544.18 *DOI: 10.15407/Surface.2025.17.118*

DIRADICAL AND MULTIRADICAL SYSTEMS AND QUANTUM-CHEMICAL METHODS FOR CALCULATING THEIR PROPERTIES

O. S. Kremen, V. V. Lobanov

Chuiko Institute of Surface Chemistry of the NAS of Ukraine,
17 Oleh Mudrak Str., Kyiv-03164, Ukraine, e-mail: kremenoksana@ukr.net

Intense interest in diradical (di- and multi-) compounds arises from their unique nonlinear optical (NLO) properties, manifested as responses to strong laser electric fields. Their NLO behavior finds numerous applications in spectroscopy, materials science, engineering, and in photon-based data collection, storage, processing, and transmission. The electronic structure of open-shell diradical systems is classified according to the magnitude of their diradical character (y) into three categories: (i) closed-shell systems (y = 0); (ii) intermediate diradical systems (0 < y < 1); and (iii) pure open-shell systems (y = 1). Due to the interactions between unpaired electrons in diradical species, they cannot simply be regarded as a joint system of two independent radical centers. A complete description of the electronic structure of diradical species requires consideration of both singlet and triplet open-shell states. Results obtained within a simple two-center model lead to the emergence of a new class of open-shell singlet systems, which are expected to surpass traditional closed-shell NLO systems. Based on this principle, practical guidelines for molecular design and optimization of diradical characteristics are proposed, thereby enhancing NLO responses through first-principles calculations performed on realistic singlet open-shell molecular systems. Computational data on fullerenes are valuable not only for the development of efficient NLO materials but also for understanding the origin of multiradical character in certain bonds within such systems. Although the studied fullerenes possess singlet ground states, their intermediate diradical character may result in narrowing of the energy gap between singlet states and higher spin multiplets. In the context of molecular magnetism, it has been shown that the main effect beyond CAS, determined by the DDCI2 method (constructed from second-order perturbation theory terms), arises from external space determinants of the 1h + 1p type and represents a fourth- and higher-order correction. This effect consists of dynamic re-polarization of ionic structures of valence bonds. Beyond the DDCI2 space, which does not provide quantitative agreement with experiment, it is necessary to account for 2h + 1p and 1h + 2p excitations. Their influence is significant and does not correspond to ligand dynamic polarization via charge transfer to the metal atom, but rather occurs through dynamic coupling of ligand-metal transition dipoles with transition dipoles of surrounding electrons, thereby increasing the effective hopping integral of dispersive origin. Within Noodleman's method, it has been demonstrated that for the generation of wave functions and matrix elements used in the calculation of higher spin multiplet energies, one may employ either the unrestricted Hartree–Fock approach or spin-polarized density functional theory. One of the advantages of broken-symmetry wave functions is that, being single-configuration wave functions, they are easily visualized. Moreover, a broken-symmetry wave function provides a weighted average of pure spin states, which are orthogonal and do not interact with the system's overall Hamiltonian. This is a powerful result that can be exploited to evaluate the energies and properties of pure spin states.

Keywords*: diradical state, diradical character, open-shell singlet states, nonlinear optical properties, fullerene diradical states, natural orbital occupation numbers, magnetic exchange constant.*

INTRODUCTION

Diradical and multiradical compounds [1–3] play an important role in molecular systems and their transformations, particularly in processes such as cycloaddition [4, 5] and chemical reactions of biological relevance, including the thermal isomerization of the retinal chromophore involved in the visual mechanism [6, 7]. In many cases, the reaction pathway may proceed through a transition state of diradical character. Typical examples include the dimerization of butadiene [4, 5] and the reaction between butadiene and ethylene [8], in which diradical transition states are assumed to be energetically competitive with aromatic ones.

The primary reason for the growing interest in diradical compounds lies in their unique nonlinear optical (NLO) properties, which arise under interaction with strong laser electric fields. NLO phenomena find numerous applications in spectroscopy, materials science, and engineering [9], as well as in photon-based data collection, storage, processing, and transmission [10–12]. Although traditional materials with large first (β) and second (γ) hyperpolarizabilities are inorganic crystals (e.g., $LiNbO_3$, KH_2PO_4), in recent decades π-electron conjugated organic molecular systems [9] have been considered as alternatives due to their stronger optical nonlinearity, faster optical response, simpler molecular design, and potentially lower processing costs compared to inorganic crystals. However, most of these systems are closed-shell, whereas studies [1–3] have emphasized that open-shell systems, particularly singlet open-shell systems, may exhibit more pronounced NLO properties. Such singlet open-shell systems possess unique physicochemical features, such as a narrow singlet–triplet gap (~0.5 eV) in long acenes with singlet ground states, high reactivity of zigzag edges [13, 14], enhanced charge-carrier mobility [15], and, in the solid state, interatomic distances shorter than the sum of the van der Waals radii of the atoms forming the bond [15, 16].

These atypical properties for singlet states are determined by the unique electronic structure of such systems, which can be characterized as open-shell or as having multiradical character [17–19]. Diradical (n = 2) or higher-order (n = 4 (tetra), 6 (hexa), …) character is not a directly observable property but represents a quantum-chemical index, originally defined as twice the weight of the double-excitation configuration in the multiconfigurational self-consistent field (MC-SCF) method [17]. In [18, 19], an approximate spin-projection scheme was proposed for evaluating diradical character (y) using broken-symmetry (BS) approaches and a single Slater determinant, i.e., within the unrestricted Hartree – Fock (UHF) or unrestricted density functional theory (UDFT) frameworks. Subsequently, diradical character was associated with "ground-state bond instability" [18]. On the other hand, excitation energies and other molecular properties are also closely related to ground-state diradical character [1, 20–22]. Analytical expressions for excitation energies and transition moments as functions of diradical character were derived using a two-center diradical model based on the two-electron valence configuration interaction (2e-VCI) method [21]. Since diradical character is a chemical index associated with ground-state bond energy and thus readily understood by chemists, such expressions are useful for developing guidelines for the design of efficient photosensitive molecular systems [23].

The electronic structure of open-shell diradical systems is classified into three categories: (i) closed-shell systems (y = 0); (ii) intermediate diradical systems (0 < y < 1); and (iii) pure open-shell systems (y = 1) [23]. Based on the analysis of purely theoretical and quantum-chemical studies, it has been found that γ, a third-order NLO property at the molecular level, exhibits strong correlation with diradical character y, referred to as "$\gamma - y$ correlation". For systems with intermediate values of y around 0.5, large γ amplitudes are observed compared to closed-shell (y = 0) and pure diradical (y = 1) systems of comparable molecular size [24]. This $\gamma - y$ correlation was confirmed by analytical expressions derived within the two-electron valence configuration interaction (2e-VCI) approach [21]. It was further illustrated by results of highly correlated *ab initio* molecular orbital (MO) calculations and unrestricted density

functional theory (UDFT) for various model and real open-shell molecular systems, such as the stretched H_2 molecule [25], twisted ethylene [24], *p*-quinodimethane [24], imidazole and triazolobenzene [26], polycyclic hydrocarbons including graphene nanoparticles [27], multinuclear transition-metal complexes [28, 29], and photochromic compounds [30].

The dependence of γ on diradical character was subsequently confirmed experimentally through high-intensity two-photon absorption (TPA) [31, 32] and third-harmonic generation (THG), typical third-order NLO properties, in several thermally stable singlet open-shell diradicaloids [33, 34] with intermediate values of *y*.

For quantitative determination of potential energy surfaces (PES) of reaction pathways involving diradical compounds, very high-level computations are required, including adequate treatment of both static and dynamic electron correlation. On the other hand, determining the relative stability of singlet and triplet states even for small molecules [35] can be a challenging task for quantum-chemical calculations. The multiplicity of unpaired electrons also complicates the design of new magnetic materials based on polyradical states [36].

According to the definition provided in the pioneering work on diradical states [1], diradical compounds are molecules with two unpaired electrons occupying two degenerate or nearly degenerate molecular orbitals. Molecules with a broken double bond can serve as convenient models of diradicals. One of the most illustrative cases is rotation around the carbon–carbon double bond in ethylene, C_2H_4 [2, 37–39]. Upon transition from a planar structure to an orthogonally twisted conformation, the bonding π- and antibonding π* orbitals of the singlet ground state of C_2H_4 become degenerate, and the single-configuration π^2 wave function is no longer suitable for describing its electronic state. Orthogonally twisted ethylene thus represents a prototype of a homosymmetric diradical [1]. Standard density functional theory (DFT) and restricted Hartree – Fock (RHF) fail to qualitatively describe the shape of the torsional barrier (the energy–torsion curve shows a cusp at 90° instead of a smooth profile) [38, 40]. To properly describe ethylene twisted by 90°, at least two configurations, π^2 and $(\pi^*)^2$, must be considered. The methylene molecule, CH_2, belongs to heterosymmetric diradicals, since the two molecular orbitals occupied by unpaired electrons have different symmetries ($1b_1$ and $3a_1$). This radical has been extensively studied to assess the reliability of quantitative *ab initio* calculations of the equilibrium geometry of the triplet state and the singlet–triplet gap ($X^3B_1 - a^1A_1$) [1, 41].

GENERAL INFORMATION ON DIRADICAL SYSTEMS

In diradicals or biradicals, two unpaired electrons strongly interact with each other [1]. These electrons usually participate in conjugation and may form either a singlet ground state (antiferromagnetic coupling) or a triplet ground state (ferromagnetic coupling) (Fig. 1) [42], in contrast to “disbiradicals”, where two unpaired electrons interact weakly or almost not at all and can be considered independent isolated radical centers [43, 44]. Diradicals are characterized by their diradical character, which is typically quantified using several different indicators. In the limit of fully degenerate frontier molecular orbitals, the values of these indicators approach 1, corresponding to a fully diradical state. However, for most diradicals, a small energy gap between the highest occupied molecular orbital (HOMO) and the lowest unoccupied molecular orbital (LUMO) ($\Delta = \varepsilon_{LUMO} - \varepsilon_{HOMO}$) is observed, and thus they can be classified as systems with partial diradical character, usually corresponding to indicator values between 0.20 and 0.80 [45].

Historically, diradicals were characterized only as intermediate structures describing the transition states of bond-breaking and/or bond-forming processes. However, as noted in [46], the introduction of steric strain into homo- or heterocycles to prevent bond formation, or substitution of carbon atoms with main-group elements, significantly stabilizes diradical states, leading to their persistence and allowing determination of the corresponding structural characteristics. Nevertheless, the modifications mentioned above reduce the diradical character, and the resulting systems are more appropriately referred to as diradicaloids [47]. Diradicaloids have found

applications in small-molecule activation, molecular switches, nonlinear optics, and spintronics [48–51].

Due to the interactions between unpaired electrons in diradical or diradicaloid species, they cannot simply be regarded as a joint system of two independent radical centers. A complete description of the electronic structure of diradical or diradicaloid species requires consideration of both singlet and triplet open-shell states [52].

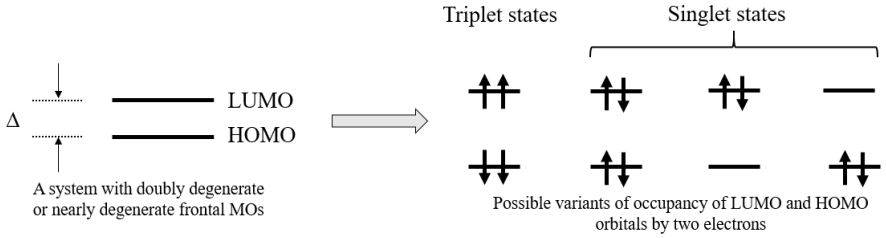

Fig. 1. Electron configurations obtained when doubly degenerate or nearly degenerate MOs ($\Delta \to 0$) are populated by two electrons. Determinants corresponding to these configurations are necessary for constructing wave functions for singlet and triplet states of diradical systems

The wave function of the triplet state of a diradical system Ψ_T can be represented as a single Slater determinant. However, when the frontier MOs are degenerate or nearly degenerate, the lowest-energy singlet wave function Ψ_S must account for several electronic configurations, resulting in its representation as a linear combination of at least two Slater determinants. In this combination, the configuration interaction (CI) coefficients c_1 and c_2 determine the contribution of each determinant to the overall singlet-state wave function of the system, where ψ_H corresponds to the HOMO and ψ_L to the LUMO:

$$\left|\Psi_T\right\rangle = \left|\psi_H \psi_L\right\rangle; \quad \Psi_S = c_1 \left|\psi_H^2\right\rangle - c_2 \left|\psi_L^2\right\rangle, \tag{1}$$

where the symbol |…> denotes a Slater determinant including only the two highest-energy orbitals, HOMO and LUMO. When $c_1 = c_2 = 1/\sqrt{2}$ the frontier orbitals ψ_H and ψ_L are degenerate, the singlet wave function Ψ_S describes an ideal diradical. As the energy gap Δ increases, the corresponding Ψ_S wave function approaches that of a classical closed-shell system, with $c_1 \to 1$ and $c_2 \to 0$, so that in the lowest-energy singlet state the dominant contribution arises from the doubly occupied HOMO.

TWO-CENTER MODEL

For a clearer representation of the diradical nature of triplet and singlet wave functions, they should be expressed in the basis of orthonormal localized atomic orbitals (AOs) $\chi_A(x)$ and $\chi_B(x)$, where orbital $\chi_A(x)$ is localized on radical center A and orbital $\chi_B(x)$ on radical center B [53] (Fig. 2), with the overlap integral equal to zero. The HOMO $\psi_H(x)$ can then be expressed as the node-free sum $\chi_A(x) + \chi_B(x)$, while the LUMO $\psi_L(x)$ is given by the $\chi_A(x) - \chi_B(x)$, containing a nodal plane:

$$\psi_H(x) = \left(\chi_A(x) + \chi_B(x)\right)/\sqrt{2}; \quad \psi_L(x) = \left(\chi_A(x) - \chi_B(x)\right)/\sqrt{2}. \tag{2}$$

Within this approach, the singlet wave function Ψ_S can be expressed as a combination of covalent Ψ_{cov} and ionic Ψ_{ion} contributions. The covalent wave function represents an electronic configuration in which each localized orbital is singly occupied, corresponding to diradical

character. The ionic component represents an electronic configuration in which one localized orbital is doubly occupied while the other remains empty, corresponding to a zwitterionic state:

$$\Psi_S = \frac{c_1 + c_2}{\sqrt{2}} \frac{1}{\sqrt{2}} \left(|\chi_A \chi_B\rangle - |\chi_B \chi_A\rangle \right) + \frac{c_1 - c_2}{\sqrt{2}} \frac{1}{\sqrt{2}} \left(|\chi_A^2\rangle - |\chi_B^2\rangle \right), \tag{3}$$

$$\Psi_S = c_{\text{cov}} \Psi_{\text{cov}} + c_{\text{ion}} \Psi_{\text{ion}},$$

where

$$c_{\text{cov}} = \frac{c_1 + c_2}{\sqrt{2}} \text{ and } c_{ion} = \frac{c_1 - c_2}{\sqrt{2}}. \tag{4}$$

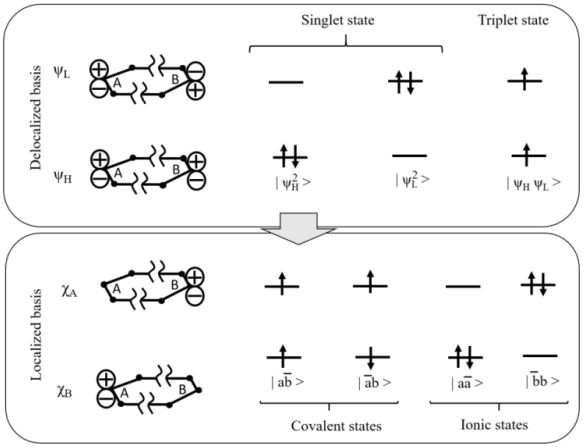

Fig. 2. Schematic representation of the consequence of the transition from the basis of diradical MOs (Ψ_H and Ψ_L) to the basis of localized AOs (χ_A and χ_B)

If $c_1 = c_2 = 1/\sqrt{2}$, $c_{\text{cov}} = 1$, $c_{\text{ion}} = 0$, and this situation corresponds to 100% diradical character. As the HOMO–LUMO gap increases, coefficient c_1 approaches 1 while coefficient c_2 tends to 0, leading to $c_{\text{cov}} = c_{\text{ion}}$. In this state, complete electron delocalization occurs within the two-orbital system, equivalent to the electronic configuration of a closed-shell system [46].

The CI coefficients c_1 and c_2 can be used for quantitative evaluation of the diradical state indicator [47]. In the literature, several types of diradical indicators have been proposed, expressed through the relative weights of covalent and ionic contributions:

$$\gamma = \sqrt{2} c_2 = c_{\text{cov}} - c_{ion}; \quad d = 2c_1 c_2 = c_{\text{cov}}^2 - c_{ion}^2; \quad \beta = 2c^2 = \left(c_{\text{cov}} - c_{ion} \right)^2. \tag{5}$$

All of these indicators (γ, d, β) effectively reflect the extent to which the relative weight of the covalent component in the singlet wave function Ψ_S exceeds the ionic contribution [54 – 56]. Thus, the higher the values of these indicators, the greater the diradical character of the system under study. For pure diradical states, these indicators approach unity, while for classical closed-shell systems they tend toward zero [45].

Natural orbital (NO) occupation numbers also serve as another theoretical measure of diradical character [57, 58]. The occupation of the lowest unoccupied natural orbital (LUNO) corresponds to the indicator β and lies between 0 and 1; the closer this value is to 1, the stronger the predicted diradical character. Conversely, the occupation of the highest occupied natural orbital (HONO) ranges from 1 to 2; the closer this value is to 1, the stronger the predicted diradical character. These NO occupation numbers can be practically calculated using relatively simple quantum-chemical methods at lower computational cost compared to CI-based approaches. A small singlet–triplet energy gap also indicates enhanced diradical character [59]. Finally, if the calculated interatomic distance A···B (where A and B are radical centers) is

elongated relative to the sum of covalent radii (typical for closed-shell molecules) but shorter than the sum of van der Waals radii, this also suggests the presence of a diradical state [46]. Introduction of bulky substituents or ring strain in heterocycles may prevent bond formation and/or lead to bond elongation.

HOMOSYMMETRIC SINGLET OPEN-SHELL STATES

A more complete picture of energy-level splitting within the two-center diradical model can be obtained by supplementing the one-electron functions $\psi_H(x)$ and $\psi_L(x)$ defined in (2) with spin functions $\alpha(\sigma)$ and $\beta(\sigma)$, where σ is the spin variable taking values $\sigma = 1/2$ and $\sigma = -1/2$. The spin function equals 1 only for $\sigma = -1/2$, while $\beta(\sigma)$ equals 1 only for $\beta(\sigma) = 0$. With this definition, $\alpha(\sigma)$ and $\beta(\sigma)$ are orthogonal and each normalized to unity. Multiplying the spatial functions $\psi_H(x)$ and $\psi_L(x)$ (depending only on the spatial coordinate *x*) by the spin functions $\alpha(\sigma)$ and $\beta(\sigma)$ yields four spin-orbitals:

$$a(x,\sigma) = \psi_H(x)\alpha(\sigma);\ \bar{a}(x,\sigma) = \psi_H(x)\beta(\sigma);\ b(x,\sigma) = \psi_L(x)\alpha(\sigma);\ \bar{b}(x,\sigma) = \psi_L(x)\beta(\sigma). \quad (6)$$

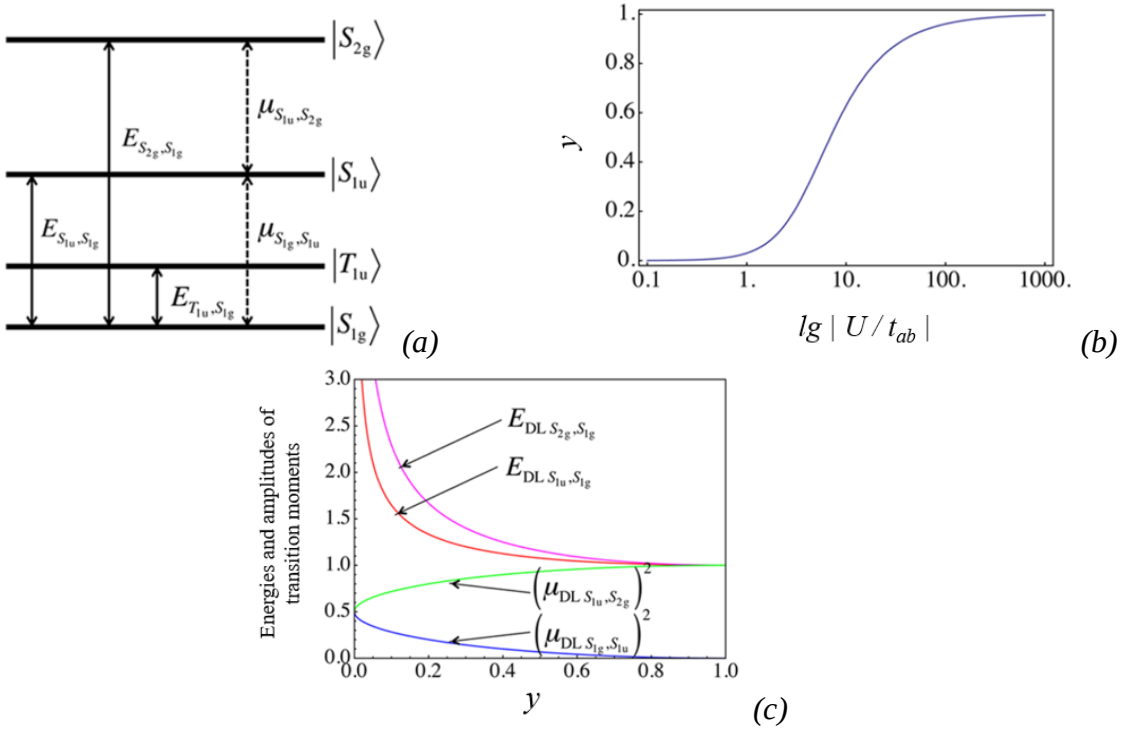

Fig. 3. Four states {$|S_{1g}\rangle$, $|T_{1u}\rangle$, $|S_{1u}\rangle$, $|S_{2g}\rangle$} of the two-site diradical model (*a*), diradical character *y* versus $|U/t_{ab}|$ (*b*), as well as diradical character dependences of dimensionless excitation energies ($E_{DL\,S1u,S1g}$ and $E_{DL\,S2g,S1g}$), squared transition moments ($(\mu_{DL\,S1g,S1u})^2$, and $(\mu_{DL\,S1u,S2g})^2$) (*c*) [36]

Using the basis of spin-orbitals defined in (6), [20, 21] obtained the energy-level diagram shown in Fig. 3*a* for the one-dimensional case of the two-center diradical model.

For the lowest-energy covalent symmetric (*g*) singlet state with energy ${}^1E_{1g}$, the wave function is given by [22]:

$$|S_{1g}\rangle = k\left(|a\bar{b}\rangle + |b\bar{a}\rangle\right) + \eta\left(|a\bar{a}\rangle + |b\bar{b}\rangle\right);\ k > \eta > 0. \quad (7)$$

The higher-energy ionic singlet antisymmetric state with energy ${}^1E_{1u}$ is described by a singlet antisymmetric (*u*) wave function:

$$|S_{1u}\rangle = \left(|a\bar{a}\rangle - |b\bar{b}\rangle\right)/\sqrt{2}. \quad (8)$$

The highest singlet symmetric ionic state with energy ${}^1E_{2g}$ is represented by a singlet symmetric function that describes the ionic state:

$$|S_{2g}\rangle = -\eta\left(|a\bar{b}\rangle + |b\bar{a}\rangle\right) + k\left(|a\bar{a}\rangle + |b\bar{b}\rangle\right);\ k > \eta > 0. \quad (9)$$

The wave function of the unique triplet covalent state with energy ${}^3E_{1u}$ has a simple form:

$$|T_{1u}\rangle = \left(|a\bar{b}\rangle - |b\bar{a}\rangle\right)/\sqrt{2}. \quad (10)$$

In [21], the following relation was derived for computing the diradical indicator *y*:

$$y = 2\xi^2 = 1 - \frac{4|t_{ab}|}{\sqrt{U^2 + 16t_{ab}^2}} = \frac{4r_t}{\sqrt{1+16r_t^2}}. \quad (11)$$

In formula (11) the following notations are used:

$$\begin{aligned} &r_t = |t_{ab}|U\ (\geq 0);\ U = U_{aa} - U_{ab} = \langle aa|\,aa\rangle - \langle aa|\,bb\rangle; \\ &t_{ab} = t_{ba} \equiv \langle a|\,f\,|b\rangle = \langle b|\,f\,|a\rangle = \langle \bar{a}|\,f\,|\bar{b}\rangle = \langle \bar{b}|\,f\,|\bar{a}\rangle, \end{aligned} \quad (12)$$

where *f* is the Fockian of the system under consideration, *U* is the effective Coulomb repulsion of electrons of the radical centers.

From (11) and (12), it follows that the indicator *y*, which defines the degree of diradical character, satisfies the conditions: $y \to 1$ for $r_t \to 0$ and $y \to 0$ for $r_t \geq 1$. These relations ensure that y takes values between 0 and 1, corresponding to closed-shell (bonding) and pure diradical (bond-breaking) states, respectively. Since *U* determines the difficulty of electron transfer between centers A and B, while $|t_{ab}|$ defines the ease of this transfer, the case $r_t \to 0$ describes complete electron localization at each center (pure diradical state $y \to 1$), whereas $r_t \geq 1$ ($|t_{ab}| \geq U$) corresponds to significant electron delocalization across both centers (stable bonding state $y \to 0$) (see Fig. 3*b*). In other words, the diradical indicator y is linked to electronic correlation through r_t. Alternatively, y can be expressed in terms of the LUNO occupation number, n_{LUNO}. Since $n_{LUNO} = 2 - n_{HONO}$, the value of $q = 1 - y = (n_{HONO} - n_{LUNO})/2$ corresponds to the "effective bond order," where n_{HONO} and n_{LUNO} are the occupancies of the bonding and antibonding natural orbitals, respectively.

Thus, the diradical character indicator y defines the degree of electronic correlation in the physical sense, while $q = 1 - y$ is the effective bond order represents the chemical interpretation [18, 21, 23, 25].

In [21], using dimensionless quantities (DL), the following expressions were obtained for excitation energies between states S_{1g}, S_{2g} and S_{1u}:

$$\begin{aligned} &E_{DL\,S_{1u},S_{1u}} = \frac{{}^1E_{1u} - {}^1E_{1u}}{U} = 1 - r_j = \frac{1}{2}\left(1 - 2r_K + \frac{1}{\sqrt{1-q^2}}\right); \\ &E_{DL\,S_{2q},S_{1g}} = \frac{{}^1E_{2q} - {}^1E_{1g}}{U} = 1 + 2(r_K - r_j) = \frac{1}{\sqrt{1-q^2}}, \end{aligned} \quad (13)$$

where

$$r_K = 2K_{ab}/U(\geq 0);\ r_J = 2J/U,\quad K_{ab} = K_{ba} = \langle ab|ba\rangle = \langle ba|ab\rangle = \langle ab|ba\rangle = \langle ba|ba\rangle. \quad (13a)$$

The parameter J has the meaning of an effective exchange integral in the Heisenberg Hamiltonian [60] for a two-center model system, $\hat{H}_{AB} = -2J\hat{S}_A\hat{S}_B$ where $\hat{S}_A$ and $\hat{S}_B$ are the spin-moment operators of radical centers A and B, respectively. The value of J is defined through the energy difference between the lowest singlet and triplet states [20, 21]:

$$2J = {}^1E_{1g} - {}^3E_{1u} = 2K_{ab} + \frac{U - \sqrt{U^2 - 16t_{ab}^2}}{2}. \quad (14)$$

Also, through the quantity q using dimensionless quantities, one can obtain useful formulas for the moments of transitions between states S_{1g} and S_{1u}; S_{1u} and S_{1g}:

$$\begin{aligned}\left(\mu_{DL\,S_{1g},S_{1u}}\right)^2 &= \left(\frac{\mu_{S_{1g},S_{1u}}}{R_{AB}}\right) = \frac{r_K - r_J}{1+2\left(r_K - r_J\right)} = \frac{1-\sqrt{1-q^2}}{2};\\ \left(\mu_{DL\,S_{1u},S_{2q}}\right)^2 &= \left(\frac{\mu_{S_{1u},S_{2q}}}{R_{AB}}\right) = \frac{1}{2}\left(1+\frac{1}{1+2\left(r_K - r_J\right)}\right) = \frac{1+\sqrt{1-q^2}}{2}.\end{aligned} \quad (15)$$

The dependencies of excitation energies and transition moments on the value of the diradical indicator y at $r_K = 0$ (the typical case) are shown in Fig. 3*c*. The transition moment between states $|S_{1g}\rangle$ and $|S_{2g}\rangle$ is equal to zero because they possess the same *g*-symmetry. As y increases, both dimensionless excitation energies (Eq. 13) approach 1, with a rapid decrease in the region of small y. Starting from $\left(\mu_{DL\,S_{1g},S_{1u}}\right)^2 = \left(\mu_{DL\,S_{1u},S_{2q}}\right)^2 = 0.5$ for $y = 0$, the excitation energy $\left(\mu_{DL\,S_{1g},S_{1u}}\right)^2$ decreases monotonically to 0, whereas $\left(\mu_{DL\,S_{1u},S_{2q}}\right)^2$ increases to 1. These changes occur because the ionic contribution of states $|S_{1g}\rangle$ and $|S_{2g}\rangle$ rangle decreases (or increases) as a function of y, while state $|S_{1u}\rangle$ rangle retains a purely ionic nature. It should be noted that real, rather than dimensionless, excitation energies depend not only on *y* but also on the amplitude *U*. Moreover, from Eq. (11) it follows that *y* increases with *U*. Therefore, as *U* grows, the excitation energy $E_{S_{1u},S_{1u}}$ decreases, reaching a stationary value, and in some cases at very large values of *U* it increases again in the region of large y [61]. Thus, excitation energies and transition moments are uniquely determined by the diradical character of the electronic ground state.

HETEROSYMMETRIC OPEN-SHELL SINGLET STATES

Heterosymmetric singlet molecular systems with open shells represent another class of compounds in which the heterosymmetry of radical centers plays an important role in the structure of their ground and excited electronic states [62]. Following the approach outlined for homosymmetric systems, in this case localized atomic orbitals AO $\chi_A(x)$ and $\chi_B(x)$ (Eq. 2) are also employed, whose linear combinations define the bonding $q(x)$ and antibonding $u(x)$ MO, represented as:

$$q(x) = \frac{1}{\sqrt{2(1+S_{AB})}}\left[x_A(x) + x_B(x)\right],\ \ u(x) = \frac{1}{\sqrt{2(1-S_{AB})}}\left[x_A(x) - x_B(x)\right]. \quad (16)$$

Here the atomic orbitals (AOs) are different, $x_A(x) \neq x_B(x)$ and their overlap is nonzero, i.e., $S_{AB} = \langle \chi_A | \chi_B \rangle$. Since the system under consideration differs somewhat from the homosymmetric case, the determination of energy levels and the corresponding wave functions introduces several new parameters, while some of those defined earlier are redefined. Thus, a parameter $h = h_{aa} - h_{bb} > 0$ is introduced, equal to the difference between the one-electron matrix elements of the core Hamiltonian, where $h_{pp} = \langle p|h(1)|p\rangle = \langle \bar{p}|h(1)|\bar{p}\rangle \leq 0$. For the heterosymmetric system, the transfer parameter is expressed through a two-electron integral; therefore, in this case, two types of transfer integrals must be considered, for example, $t_{ab(aa)} = \langle a\bar{b}|\hat{H}|a\bar{a}\rangle$ and $t_{ab(bb)} = \langle a\bar{b}|\hat{H}|b\bar{b}\rangle$, which are not equal because $\langle ab|aa\rangle \neq \langle ab|bb\rangle$. An averaged transfer integral $t_{ab} = (t_{ab(aa)} + t_{ab(bb)})/2$, is introduced, as well as quantities U_a and U_b, according to the relations $U_a = U_{aa} - U_{ab} + X$ $U_b = U_{bb} - U_{ab} - X$ given in [62], where $X = \sum_c^{core} \left[2(U_{ac} - U_{bc}) - (K_{ac} - K_{bc})\right]$f or homosymmetric molecular systems, and $U_a (= U_b)$ describes the effective Coulomb repulsion, i.e., the difference between the one-center Coulomb integrals [$U_{aa} (= U_{bb})$]and the two-center integral (U_{ab}). By employing the averaged effective Coulomb repulsion $U\left[= (U_a + U_b)/2\right]$, dimensionless parameters were introduced in [62].

$$\frac{|t_{ab}|}{U} = r_t (\geq 0); \quad \frac{2K_{ab}}{U} = r_K (\geq 0); \quad \frac{h}{U} = r_h (\geq 0); \quad \frac{U_a}{U_b} = r_U (\geq 0); \quad \frac{|t_{ab(aa)}|}{|t_{ab(bb)}|} = r_{tab} (\geq 0). \tag{17}$$

The last three parameters determine the degree of heterosymmetry in electron distribution, when greater occupancy on center A compared to center B is caused by an increase in $r_h (\geq 0)$ or a decrease in $r_U (\geq 0)$ or $r_{tab} (\geq 0)$. Since the natural orbitals (NOs) χ_A and χ_B are well localized on centers A and B, it is assumed that the difference between $t_{ab(aa)}$ and $t_{ab(bb)}$ is negligible, i.e., $r_{tab} \sim 1$, compared to the difference between h_{aa} and h_{bb}, and between U_{aa} and U_{bb}. Here, variation of r_h from 0 to 2 is considered while keeping (r_U, r_{tab}) = (1, 1) for simplicity, which corresponds to the situation where heterosymmetry is mainly governed by the difference in ionization potentials of atoms at centers A and B. As an alternative to r_t, it is convenient to introduce the symbol of pseudodiradicality y_S [62]:

$$y_S = 1 - \frac{4r_t}{\sqrt{1 + 16r_t^2}}, \tag{18}$$

which can be reduced to the diradicality indicator for the homosymmetric system (Eq. 11), i.e., with parameters (r_h, r_U, r_{tab}) = (0, 1, 1). The diradical character of heterosymmetric systems is denoted as y_A, which is a function of (r_t, r_K, r_h, r_U, r_{tab}). Solving the eigenvalue equation within the two-electron valence configuration interaction (2e-VCI) method [21] yields eigenvalues and eigenvectors as functions of (r_t, r_K, r_h, r_U, r_{tab}) or (y_s, r_K, r_h, r_U, r_{tab}). The eigenvalues and eigenvectors are described by the set {j} = {T, g, k, f} (T: triplet state; g, k, f: singlet states) and {$C_{a\bar{b},j}$, $C_{b\bar{a},j}$, $C_{aa,j}$, $C_{b\bar{b},j}$}, respectively:

$$\Psi_j = C_{a\bar{b},j}|a\bar{b}\rangle + C_{b\bar{a},j}|b\bar{a}\rangle + C_{a\bar{a},j}|a\bar{a}\rangle + C_{b\bar{b},j}|b\bar{b}\rangle. \tag{19}$$

Using molecular orbitals (g and u) (see Eq. 16), an alternative basis set $\{|G\rangle = |g\bar{g}\rangle; |S\rangle = \left[|g\bar{u}\rangle - |\bar{g}u\rangle\right]/2; |D\rangle = |u\bar{u}\rangle\}$ can be constructed for singlet states in the form

of determinants describing the ground state, singly excited, and doubly excited configurations. This allows one to obtain eigenvalues and eigenvectors by solving the eigenvalue equation in the valence configuration interaction representation [62]. For example, the ground state is represented by the wave function:

$$\left|\Psi_g\right\rangle = \xi\left|G\right\rangle + \eta\left|S\right\rangle - \zeta\left|D\right\rangle, \tag{20}$$

with the normalization condition: $\xi^2 + \eta^2 + \zeta^2 = 1$. Comparing Eqs. (19) and (20), the following relations are obtained:

$$\xi = C_{a\bar{b},g} + \left(C_{a\bar{a},g} + C_{b\bar{b},g}\right)/2, \quad \eta = \left(C_{a\bar{a},j} - C_{b\bar{b},j}\right)/\sqrt{2}, \qquad \zeta = C_{a\bar{b},g} - \left(C_{a\bar{a},g} + C_{b\bar{b},g}\right)/2. \tag{21}$$

From the eigenfunctions, one can trace the evolution of covalent (P_C) and ionic (P_I) occupancies of the three singlet levels {*g*, *k*, *f*} as a function of r_h,, which are given by $P_C = \left|C_{a\bar{b},i}\right|^2 + \left|C_{b\bar{a},i}\right|^2$ and $P_I = \left|C_{a\bar{a},i}\right|^2 + \left|C_{b\bar{b},i}\right|^2$ for state *j*. Figure 4*a* shows the dependencies of P_C and P_I on r_h for $r_K = 0$ and various values of y_S (or r_t). P_C and P_I exhibit mirror-like changes with respect to r_h (with $P_C = P_I = 1/2$, since $P_C + P_I = 1$). As seen in Fig. 4*a*, in the ground state P_C decreases (while P_I increases) with r_h, so that the curves intersect at $r_h \sim 1$ for $y_S = 0.6$. In contrast, in the first excited state (Fig. 4*b*), P_I decreases from 1 (while P_C increases from 0), and again P_I and P_C intersect near $r_h = 1.0$. Specifically, for intermediate values of y_S, increasing r_h induces inversion of the dominant electronic configurations (neutral/ionic) in states *g* and *k* around $r_h = 1$, which confirms the reduction of y_A to 0 for $r_h > 1$, as shown in Fig. 4*a*. In state *f* (Fig. 4*c*), P_I slightly increases (while P_C slightly decreases) with r_h, although at any r_h the state remains nearly purely ionic. The relation $P_C = P_I$ at $r_h \sim 1$ for $y_S > 0$ can be qualitatively explained by the fact that h (= $h_{bb} - h_{aa}$) ~ U corresponds to the situation where the attractive and repulsive energies between a pair of electrons χ_A and χ_B are equal, which equalizes P_C with P_I in the case of a small transfer integral (realized for $y_S > 0$).

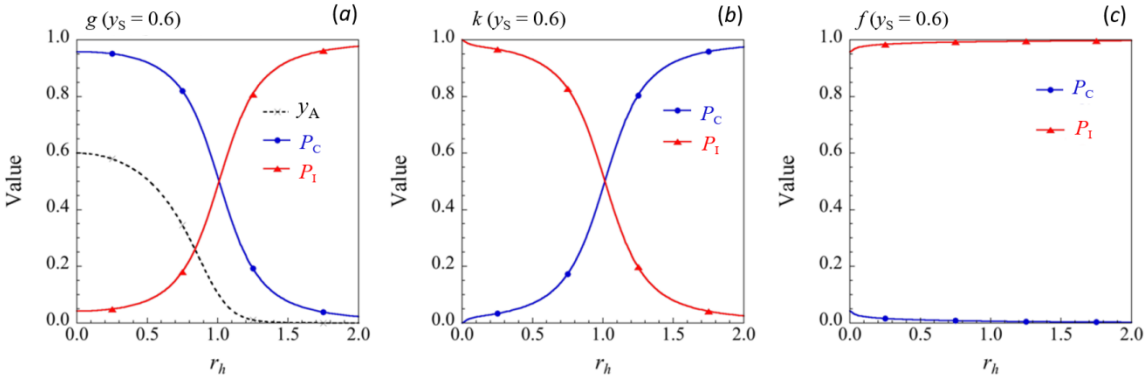

Fig. 4. r_h dependences of P_C and P_I in state *g*, *k*, and *f* for $y_S = 0.6$ (*a*–*c*). The evolution of y_A (state *g*) as a function of r_h is also displayed [36]

Next, the dependence of heterosymmetry (r_h) on the diradicality index y_A, defined through the occupation number of the lowest unoccupied natural orbital n_{LUNO}, is considered. Using Eq. (18), the following relation for y_A was obtained [62]:

$$y_A = n_{LUNO} = 1 - \left|\xi - \zeta\right|\sqrt{2 - (\xi - \zeta)^2}. \tag{22}$$

For heterosymmetric systems, Eq. (22) reduces to the conventional definition of twice the weight of the double-excitation configuration [61]:

$$y_A = y_S = 2\zeta^2 . \tag{23}$$

By employing Eqs. (21) and (22), the diradical character y_A can also be expressed as a function of natural orbital (NO) coefficients [62, 63].

$$y_A = 1 - \left| C_{a\bar{a},g} - C_{b\bar{b},g} \right|^2 \sqrt{2 - \left(C_{a\bar{a},g} - C_{b\bar{b},g} \right)^2} . \tag{24}$$

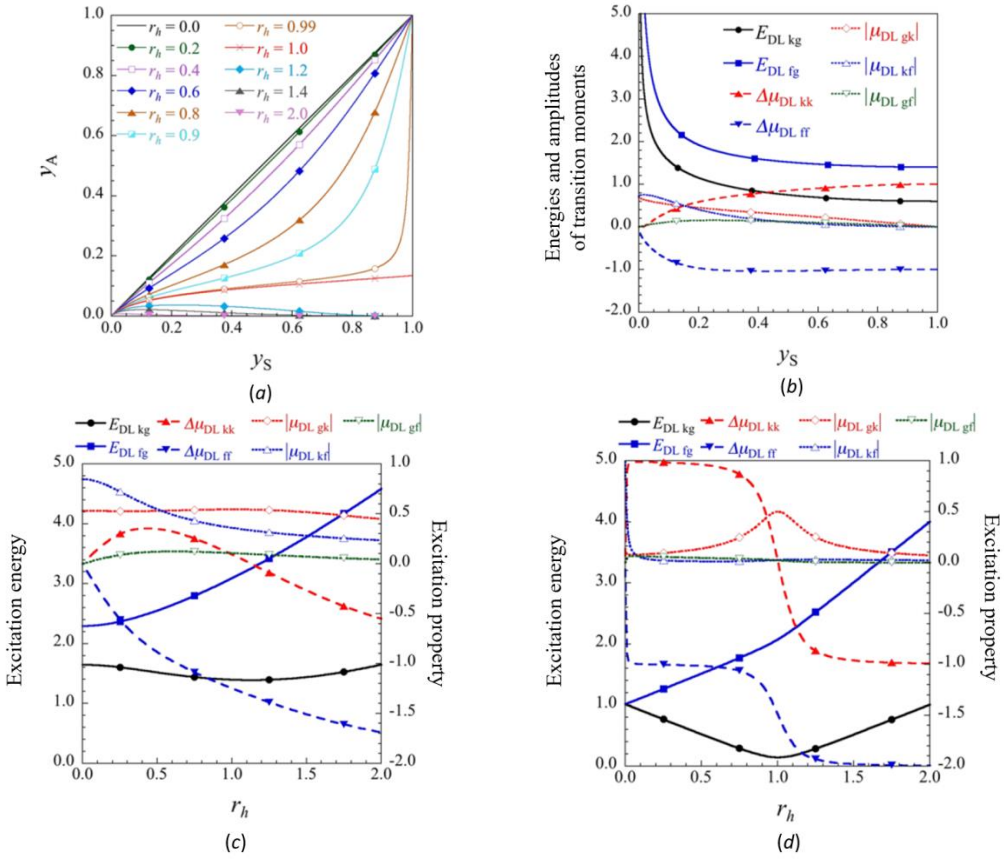

Fig. 5. y_S versus y_A plots for r_h = 0.0–2.0 (*a*), and y_S dependences of dimensionless excitation energies $E_{DL\,ij}$, transition moment amplitudes $|\Delta\mu_{DL\,ij}|$ and dipole moment differences $\Delta\mu_{DL\,ii}$, where i = *g*, *k*, and *f*, for r_h = 0.4 (*b*). Asymmetricity (r_h) dependences of the dimensionless excitation energies and properties for different pseudodiradical characters y_S = 0.1 (*c*) and 0.8 (*d*) [36]

For symmetric systems, this equation indicates that the ionic configuration with heterosymmetric electron distribution $\left(\left| C_{a\bar{a},g} \right| \neq \left| C_{b\bar{b},g} \right| \right)$ reduces the diradical character y_A; for example, y_A = 0 when $C_{a\bar{a},g}$ = 1 and $C_{b\bar{b},g} = C_{a\bar{b},g} = C_{b\bar{a},j} = 0$. Fig. 5*a* shows the dependence between y_S (Eq. 18) and y_A (Eqs. 22 and 24) for heterosymmetry at values of r_h ranging from 0.0 to 2.0. The index y_A is systematically smaller than y_S, particularly in the intermediate region of variation of y_S with increasing r_h. It was also found that for y_S = 1, y_A = 1 when r_h < 1, and an exchange of the dominant configuration (covalent/ionic) occurs in state *g* between r_h < 1 and r_h > 1 for y_S > 0.

The dependencies of dimensionless excitation energies $\left[E_{DL,ij} = \left(E_i - E_j \right) / U \right]$, transition moment amplitudes $\left| \mu_{DL,ij} \right| = \left| \mu_{ij} \right| / R_{BA}$, and dipole moment differences $\left| \Delta\mu_{DL,ij} \right| = \left(\mu_{ii} - \mu_{gg} \right) / R_{BA}$ as functions of y_S at r_h = 0.4 are shown in Fig. 5*b* [62, 63]. These dependencies were obtained under the assumption that $(a|r_1|b) \sim 0$, since orbitals *a* and *b* are well localized on each center

and their overlap is, by definition, zero. The dependencies of these quantities on y_S at $r_h = 0$ (only the homosymmetric system) were already shown in Fig. 3*a*, where $|S_{1g}\rangle = g$, $|S_{1u}\rangle = k$, and $|S_{2g}\rangle = f$ denote singlet states. When $r_h = 0.4$, with increasing y_S, the amplitudes $\Delta\mu_{DLkk}$ (positive) and $\Delta\mu_{DLff}$ (negative) increase. These differences in dipole moments indicate that the polarizations in states *g* and *k* have the same direction (from A to B), opposite to that in state *f*. Unlike the homosymmetric case ($r_h = 0$), both $|\mu_{DL,gk}|$ and $|\mu_{DL,kf}|$ excitation energies decrease to zero with increasing y_S (Fig. 3*a*). Finally, both excitation energies $E_{DL,fg}$ and $\mu_{DL,gk}$ decrease with y_S, although they are larger and smaller, respectively, than in the symmetric case ($r_h = 0$). Indeed, $E_{DL,kg} = 1 - r_h$ and $E_{DL,fg} = 1 + r_h$ at $y_S = 1$ [62, 63]. As seen in Fig. 5, and when $r_h > 1$, the dominant configurations exchange between states *g* and *k*, leading to a change in the sign of $\Delta\mu_{DL,kk}$ at $r_h \sim 1$ ($\Delta\mu_{DL,kk} > 0$ for $r_h < 1$ and $\Delta\mu_{DL,kk} < 0$ for $r_h > 1$), and for $r_h > 1$. For $r_h > 1$, its amplitude increases with y_S due to the enhanced contribution of the diradical (ionic) configuration in state *k* (or *g*). Analytically, it was also established that for $y_S = 1$ and $r_h > 1$, $E_{DL,fg} = 2r_h$ and $E_{DL,kg} = r_h - 1$, which causes an increase in $E_{DL,kg}$ after reaching a minimum at $r_h \sim 1$, while $E_{DL,fg} = 2r_h$ continues to increase with r_h (see Fig. 5*c*, *d*). On the other hand, for $r_h \sim 1$, the excitation energy $E_{DL,kg}$ decreases to zero with increasing y_S, while the transition moment $\Delta\mu_{DL,kk}$ remains close to zero, and the dipole moment difference $|\mu_{DL,gk}|$ is nearly constant (and nonzero) across the entire range of y_S. This reflects the equal weight of covalent and ionic configurations in both states, as shown in Fig. 3.

Further, in [62, 63], the dependence of excitation energies and excited-state properties on r_h was investigated for different values of pseudodiradical character $y_S = 0.1$ and 0.8 (Fig. 5*c*, *d*). In the case of $y_S = 0.1$, the excitation energy $E_{DL,kg}$ exhibits a shallow minimum at $r_h \sim 1$, while another excitation energy $E_{DL,fg}$ increases with r_h. The transition moment $|\mu_{DL,gk}|$ remains close to 0.5, whereas the dipole moment difference $|\mu_{DL,kf}|$ decreases with r_h. The increase followed by a decrease of $\Delta\mu_{DL,kk}$ as a function of r_h, positive for $r_h < 1$ and negative for $r_h > 1$, reflects the exchange of dominant covalent and ionic configurations around $r_h \sim 1$, as shown in Fig. 5. With increasing y_S, the rapid change $\Delta\mu_{DL,kk}$ from positive to negative values (together with a significant change in amplitude), maximization of one transition moment $|\mu_{DL,gk}|$ and minimization of another $E_{DL,kg}$ at $r_h \sim 1$, are features that determine the dependence of γ on r_h for heterosymmetric diradical systems [62, 63].

Summarizing the results of the two-center diradical model, it should be noted that within the valence configuration interaction scheme, recommendations have been proposed for the design of molecular systems with singlet open-shell ground states that exhibit remarkable nonlinear optical (NLO) properties. In this scheme, the concept of diradical character *y*, a chemical index reflecting bond weakness in the electronic ground state, allows classification of singlet open-shell molecular systems into three categories: (i) closed-shell systems ($y = 0$), (ii) intermediate diradical systems ($0 < y < 1$), and (iii) pure open-shell systems ($y = 1$). Within the 2e-VCI framework, molecular properties (excitation energies, transition dipole moments, dipole moments, and second hyperpolarizability) for four-electron states are expressed as functions of diradical character, which is useful for understanding photochemical properties and deriving structure–property relationships in open-shell molecular systems. It has been demonstrated that

the second hyperpolarizability is enhanced in the intermediate region of diradical character compared to other regimes. This principle also extends to the first hyperpolarizability β for asymmetric singlet open-shell systems. These results lead to the emergence of a new class of singlet open-shell systems expected to surpass traditional closed-shell NLO systems. Based on this principle, practical guidelines have been proposed for molecular design and optimization of diradical characteristics, and consequently for enhancing NLO responses, using first-principles calculations performed on realistic singlet open-shell molecular systems. These guidelines are supported by the synthesis of thermally stable singlet open-shell systems exhibiting enhanced third-order NLO properties, such as two-photon absorption cross-sections. In addition to large responses, these compounds are promising candidates for NLO switches, whose properties can be modified by external stimuli [64]. For example, switching from a singlet state to a higher-multiplet state leads to a sharp decrease in hyperpolarizability, which may serve as a theoretical basis for designing compounds with magnetically controlled NLO properties or spin-state sensors [26, 65]. Among the strategies for achieving intermediate diradical states that show higher efficiency in producing large γ-responses, the following should be noted: (i) introduction of asymmetry through donor/acceptor substitution or application of an external static electric field [66]; (ii) increasing molecular size by modifying the topology of the periphery; (iii) substitution of carbon atoms at radical centers with heavy main-group elements [67, 68]; (iv) construction of supramolecular systems with tuned planar bonds and specific chemical doping; (v) creation of one-dimensional chains of transition-metal atoms [69, 70]. Singlet open-shell systems are also of interest from the viewpoint of multifunctionality due to their magnetic interactions or half-metallicity, i.e., spin-dependent electrical conductivity [71].

DIRADICAL MOTIFS OF FULLERENES

To establish new correlations between structure and NLO properties of fullerenes arising from their possible open-shell electronic configurations, the relationship between diradical character (y_i) and the second hyperpolarizability (longitudinal component, γ_{zzzz}) was investigated in [72] for several fullerenes, including C_{20}, C_{26}, C_{30}, C_{36}, C_{40}, C_{42}, C_{48}, C_{60}, and C_{70}, using the broken-symmetry density functional theory (BS-DFT) method. It was found that large differences in equilibrium geometry and topology of fullerenes significantly affect the diradical character of each system. Based on their varying diradical character, these fullerenes were divided into three distinct groups according to the parameter y_i. According to the obtained data, closed-shell fullerenes include C_{20}, C_{60}, and C_{70}, whereas C_{26}, C_{36} and C_{30}, C_{40}, C_{42}, and C_{48} correspond to radical and intermediate open-shell compounds, respectively. Direct calculations showed that enhancement factors γ_{zzzz} between C_{30}/C_{36} and C_{40}/C_{60} are 4.42 and 11.75, respectively, despite the smaller size of the π-conjugated domain in C_{30} and C_{40} compared to C_{36} and C_{60}. Higher values of γ_{zzzz} were obtained for other fullerenes with intermediate diradical character, consistent with the results of the two-center diradical model [21].

The diradical character γ values of all selected fullerenes were calculated using the LC-UBLYP/6-31G* method (long-range corrected density functional theory) with a range-separation parameter m = 0.33. In [73], it was established that using m = 0.33 reproduces excitation energies, transition properties, and responses of various closed-/open-shell systems. For example, LC-UBLYP was found to semi-quantitatively reproduce γ values of several open-shell molecules previously calculated using highly correlated post-UHF methods, namely the spin-unrestricted coupled-cluster method (UCCSD) [73]. Since diradical character reflects bond instability, multiradical systems are characterized by multiple diradical characters (y_i) with nonzero values. Remarkably, the distribution of nonzero y_i values in the orbital space $i > 0$ indicates that the system possesses multiradical character (extending beyond the *d*-radical) for

example, $y_0 = y_1 = 1$ means that the system as a whole exhibits a purely tetraradical character [74–76]. Here, diradical character (y_i associated with the highest occupied natural orbital ($HONO-i$) and lowest unoccupied natural orbital ($LUNO+i$), where $y = 0.1$ and etc., is defined by natural orbital (n_i) (NO) occupation numbers, calculated using LC-UBLYP/6-31G* according to Eq. (25) [75–77]:

$$y_i = n_{LUNO+1} - n_{HOMO-1}, \tag{25}$$

where y_i ranges from 0 (closed-shell) to 1 (pure diradical). Thus, diradical character, which must equal 0 or 1 in spin-restricted single-determinant methods such as RHF or RDFT, can take fractional values in spin-unrestricted schemes such as UHF or UDFT.

Indeed, within the different-orbitals-for-different-spins approach, the wave function can be expanded in a restricted configuration interaction form, leading to fractional occupation numbers distinct from 0, 1, or 2. For example, in the H_2 model, LUNO occupation increases from 0 to 1 with increasing internuclear distance [78], corresponding to the degree of mixing of antibonding LUNO and bonding HONO orbitals in the singlet ground-state wave function. In MCSCF theory, diradical character was originally defined as twice the weight of the double-excitation configuration in the singlet ground state [79], but in unrestricted single-determinant schemes (UHF, UDFT) it is formally expressed by Eq. (25) [75]. The definition and physical meaning of diradical character have been discussed in several studies in connection with odd-electron densities and spin-dependent densities [77, 80, 81], which cannot be determined experimentally but represent the number and distribution of unpaired electrons. Calculated odd-electron densities provide useful and illustrative information about open-shell character and its influence on fullerene response properties [76, 77]. The odd-electron density describing spatial distribution in N-electron singlet systems is given by Eq. (26), where $d^{y_i}(\mathbf{r})$ denotes the one-electron density corresponding y_i to orbital $HONO-i$, and $LUNO+i$ are the occupation numbers of the respective NOs:

$$d(\mathbf{r}) = \sum_{i=0}^{N/2-1} \left[n_{HONO-i} \varphi^*_{HONO-i}(\mathbf{r}) \varphi_{HONO-i}(\mathbf{r}) + n_{LUNO+i} \varphi^*_{LUNO+i}(\mathbf{r}) \varphi_{LUNO+i}(\mathbf{r}) \right] = \sum_{i=0}^{N/2-1} d^{y_i}(\mathbf{r}). \tag{26}$$

The derivation of this equation is given in [76].

From [72], several important conclusions can be drawn: 1) The unique topology of fullerene systems strongly influences the diradical character of each fullerene, explained by HOMO–LUMO gaps, bond-length alternation, and distributions of odd-electron and spin densities; 2) different fullerenes exhibit distinct tendencies in their diradical character y_i, i.e., closed-shell ($y_i = 0$), intermediate open-shell ($0 < y_i < 0$), and nearly pure open-shell ($y_i \cong 1$), reflecting their diverse topological features. 3). The semi-quantitative origin of multiracial properties was traced using odd-electron densities and resonance forms of various fullerenes, applying Clar's sextet rule [82]. 4) regardless of differences in π-conjugation size, γ_{zzzz} values were significantly larger in fullerenes with intermediate diradical character than in closed-shell or pure open-shell systems, consistent with previous results from the two-center diradical VCI model [21].

The obtained results are useful not only for the development of efficient NLO materials but also for understanding the origin of multiradical character in such systems and its correlation with γ. Although the studied fullerenes possess singlet ground states, their intermediate diradical character may lead to narrowing of the energy gap between singlet states and higher-multiplet states. Furthermore, it is predicted that γ values of open-shell singlet molecules with intermediate diradical

character will be significantly reduced upon spin-state conversion from singlet to the highest possible spin states [83–85]. Considering these predictions and the obtained results, it can be expected that these di-/multiradical fullerenes will be promising candidates for new multifunctional molecular switches exploiting nonlinear optical and molecular magnetic effects.

MOLECULAR MAGNETISM AND ITS CONNECTION TO DIRADICAL STATES

Molecular and solid-state magnetism attracts increasing interest in organic and organometallic chemistry, as well as in materials science [86–88]. Such systems are characterized by the presence of unpaired electrons, usually localized on metal ions. The material properties are determined by magnetic interactions between unpaired electrons on neighboring centers, defined by the exchange coupling constant J. For two-center systems with one unpaired electron $m_s = \pm 1/2$ on each center, the exchange constant $J = E^1 - E^3$ (where E^1 and E^3 are the energies of the singlet and triplet levels, respectively) is negative for a singlet ground state (antiferromagnetism) and positive for a triplet ground state (ferromagnetism). The exchange constant J is usually very small, ranging from a few hundred to several cm^{-1}, and its calculation represents a rather challenging task. Quantum chemistry can be successfully applied for its evaluation. In most studies, density functional theory (DFT) has been employed, primarily with the B3LYP exchange–correlation functional [89–91], using Noodleman's broken-symmetry (BS) approximation [92], in which magnetic coupling is estimated from the energy difference between the unrestricted (spin-polarized) highest multiplet and the energy defined by the BS determinant. Although this procedure is useful, particularly for predicting or analyzing trends in magnetostructural correlations, it suffers from two drawbacks: dependence on the multi-parametric exchange–correlation functional V_{xc}, and problems arising from contamination by higher multiplets, which is especially significant for BS solutions.

In *ab initio* methods employing the exact Hamiltonian, these difficulties can be overcome provided that all relevant physical effects are included in the calculations, leading to good agreement with experiment. Among the most accurate methods is nonorthogonal configuration interaction (NOCI) [93], which considers a very limited number of configurations, including states accounting for charge transfer from ligand to metal [94, 95]. However, this method requires special orbital optimization for each valence-bond (VB) configuration and is therefore rarely applied. Recently, the multiconfigurational CASPT2 (Complete Active Space Second-Order Perturbation Theory) method has been widely used to compute exchange constants *J*. CASPT2 allows accurate description of strongly correlated electronic systems encountered in photochemistry and transition-metal chemistry. It is based on a reference CASSCF (Complete Active Space Self-Consistent Field) calculation, which defines a multielectron multiconfigurational wave function, followed by Rayleigh–Schrödinger perturbation theory to account for electron correlation effects. A distinctive feature of this two-step methodology is its computational efficiency compared to more elaborate methods and its ability to generate pure spin states. A significant problem, however, is the possible presence of intruder states, when nonphysical states become energetically close to the reference state. This can be mitigated by techniques such as level shifting and the introduction of the multistate CASPT2 (MS-CASPT2) formalism. Inclusion of second-order perturbation terms yields satisfactory results provided that the variational active space is sufficiently large and properly chosen [96–98]. For evaluation of vertical energy differences, an alternative CI methodology – Differential Configuration Interaction (DDCI) [99] was developed. DDCI has been successfully applied in a wide range of studies concerning molecular [100, 101] as well as solid-state magnetic materials [102,103]. For values of $J \sim 100$ cm^{-1}, the typical error is less than 10 cm^{-1}. The definition of the DDCI space is based on inclusion of second-order terms of quasi-degenerate perturbation theory, as shown in [99, 104]. The second-order perturbative approach has the advantage of decomposing the final value of *J* into contributions from different physical mechanisms [105], such as direct exchange,

Anderson's antiferromagnetic (kinetic exchange) contribution, spin polarization, etc. However, second-order perturbative expansions are not numerically reliable due to convergence problems and arbitrariness in the choice of the zero-order Hamiltonian. In the DDCI method, exact diagonalization is employed, thereby improving accuracy, though analysis of the various physical mechanisms determining exchange becomes less straightforward.

Nevertheless, the benefit of such rigorous analysis is undeniable, as it allows verification of qualitative models often used a posteriori and in molecular design of new materials [86]. In [106], it was shown that numerical accuracy (using large basis sets and extended CI expansions) can be combined with analysis in terms of physical contributions. Four different antiferromagnetic systems were considered, each involving two electrons on two Cu(d^9) centers: complexes $[Cu_2Cl_6]^{2-}$, $[Cu_2(\mu\text{-}N_3)_2(NH_3)_6]^{2+}$, $Cu_2(\mu\text{-}CH_3COO)_4(H_2O)_2$, and the Cu_2O_7 cluster, a model of the perovskite La_2CuO_4. In [106], computational details were described, theoretical justification of the results was provided, and the roles of different contributions were analyzed using natural orbitals instead of Hartree–Fock triplet orbitals.

Each of the four complexes (Fig. 6) contains two Cu(d^9) centers connected by different ligands occupying nonequivalent relative positions. The authors of [106], in the case of the $[Cu_2Cl_6]^{2-}$ ion, focused on the planar structure, where each Cu atom has square-planar coordination and carries its unpaired electron in a d_{xy}-type orbital (Fig. 7*a*).

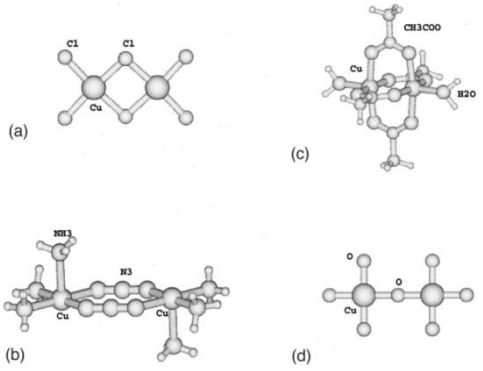

Fig. 6. Schematic representation of the four models considered: (a) the $[Cu_2Cl_6]^{2-}$, complex, in a planar geometry; (b) the $[Cu_2(\mu\text{-}N_3)_2(NH_3)_6]^{2+}$ complex with end-to-end bridging azido ligands; (c) $Cu_2(\mu\text{-}CH_3COO)_4(H_2O)_2$ complex; (d) the Cu_2O_7cluster [106]

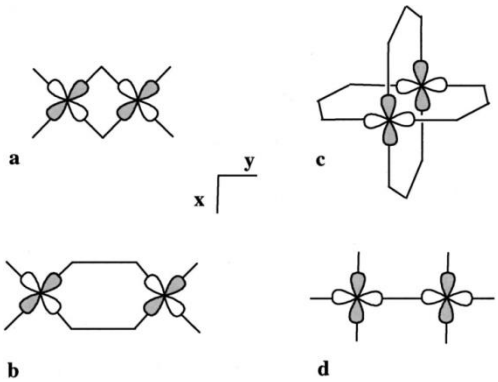

Fig. 7. Relative orientation of the magnetic orbitals in: (a) the $[Cu_2Cl_6]^{2-}$, complex, in a planar geometry; (b) the $[Cu_2(\mu\text{-}N_3)_2(NH_3)_6]^{2+}$ complex with end-to-end bridging azido ligands; (c) $Cu_2(\mu\text{-}CH_3COO)_4(H_2O)_2$ complex; (d) the Cu_2O_7cluster [106]

The experimentally established planar structure of this complex belongs to the point group C_i, but is only slightly distorted compared to the D_{2h} structure considered in [106]. A similar situation is observed in the $[Cu_2(\mu\text{-}N_3)_2(NH_3)_6]^{2+}$ complex (Fig. 6*b*), with square-pyramidal coordination of the Cu centers, each bearing a d_{xy}-type orbital (Fig. 7*b*). The Cu–Cu distance in this complex is 5.19 Å, larger than in $[Cu_2Cl_6]^{2-}$, where the distance is 3.44 Å, but the magnetic exchange constant in the former case is an order of magnitude greater than in the latter, indicating that bridging $(N_3)^-$ groups play a decisive role in magnetic exchange interactions. In the $Cu_2(\mu\text{-}CH_3COO)_4(H_2O)_2$ molecule (Fig. 6*c*), the Cu atoms also have square-pyramidal coordination but are located in parallel planes connected by four bidentate acetate ligands, separated by only 2.64 Å.

Each Cu atom carries an unpaired electron in the $d_{x2\text{-}y2}$ orbital (Fig. 7*c*). In the calculations, the experimental geometry of C_i symmetry was employed. The last system considered represents a model of the antiferromagnetic perovskite La_2CuO_4. It consists of a Cu_2O_7 cluster (Fig. 6*d*) embedded in a set of point charges simulating the Madelung field of the

La_2CuO_4 lattice. The unpaired electron resides in the $d_{x2\text{-}y2}$ orbital (Fig. 7*d*), but unlike the previous models, the Cu atoms are connected by only a single oxygen ligand.

Several qualitative models [107,108] were proposed to interpret the physical factors determining magnetic interactions. Preliminary analysis showed that the magnitude of the magnetic exchange constant J can be represented as the sum of two opposing contributions, where $J = J_F + J_{AF}$, with J_F and J_{AF} denoting the ferromagnetic and antiferromagnetic contributions, respectively. The J_F term corresponds to direct exchange between unpaired (magnetic) orbitals (always ferromagnetic), while the J_{AF} term is assumed to arise from delocalization effects, which can occur only in the singlet state (thus antiferromagnetic). This contribution is sometimes referred to as kinetic exchange. Such interpretations follow from the orthogonal VB model [107], the nonorthogonal VB model [108], or the valence configuration interaction (VCI) model [109]. In these models, two unpaired electrons are considered, each localized on one of the two centers.

Application of models [107] and [109] yielded the following expression for the magnetic exchange constant J:

$$J = 2K_{ab} - \frac{4t_{ab}^2}{U}, \tag{27}$$

where the expressions K_{ab}, U and t_{ab}^2 for J_F and J_{AF} are given by relations (12) and (13*a*).

Refinement of models [107] and [109] is possible by considering electron exchange between metal centers in systems of the type A$^{\bullet}$–L–B$^{\bullet}$. For simplicity, the ligand orbitals are restricted to a single doubly occupied orbital *l*. Two neutral VB determinants can be represented as shown in Scheme 1.

Scheme 1

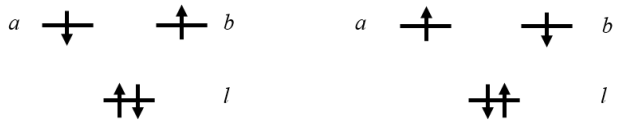

In addition to the direct interaction discussed above, an indirect interaction is also possible, which occurs through a charge-transfer process from the ligand to the metal, as illustrated in Scheme 2.

Scheme 2

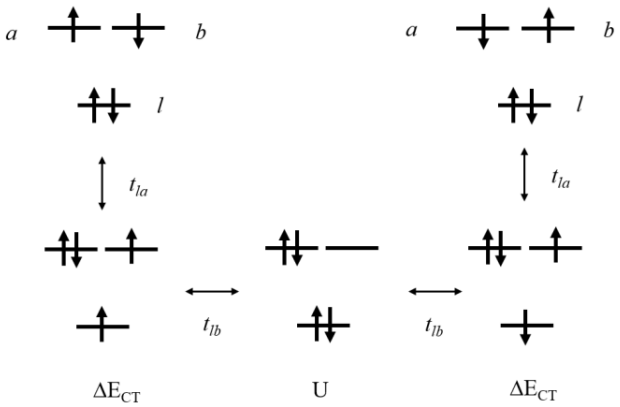

where ΔE_{CT} is the excitation energy (thus positive) associated with charge transfer from the ligand to the metal (A^-–L^+–$B^{\bullet}$). Clearly, there exists an equivalent contribution involving the intermediate state ($A^{\bullet}$–L^+–B^-).

As a result, the corresponding additional contribution to the magnetic exchange constant *J* is given by the formula:

$$J = \leftarrow -\frac{4t_{la}^2 t_{lb}^2}{\Delta E_{CT}^2 U}, \tag{28}$$

and is usually interpreted as superexchange. The contribution of successive charge-transfer processes through the ligand can be incorporated into an effective hopping integral:

$$t_{ab}^{ef} = t_{ab} - \frac{t_{la} t_{lb}}{\Delta E_{CT}}, \tag{29}$$

and for small values of t_{ab} we obtain:

$$J = 2K_{ab} - \frac{4\left(t_{ab}^{eff}\right)^2}{U}, \tag{30}$$

which again reduces to Eq. (27). In principle, other mechanisms can also be considered, proceeding through intermediate states involving double charge transfer (A^{-}–L^{++}–B^{-}) with relative energy DE_{2CT}, which may also contribute to *J*, leading to:

$$J = \leftarrow -\frac{8t_{la}^2 t_{lb}^2}{\Delta E_{CT}^2 \Delta E_{2CT}}. \tag{31}$$

This double electron transfer from ligand to metal is known in solid-state physics as the Goodenough mechanism [110]. Since the relative energy of the double ionic structure Δ*ECT* is certainly larger than *U*, it can be assumed that this mechanism contributes only negligibly to *J*, although in some cases it should be taken into account [110].

Results of calculations within the models [107,109] (2e/2MO) CASCI for the four model complexes considered showed that the ROHF orbitals of the triplet state and the singlet state ($2e^{-}$/2MO) CASSCF are practically identical. The parameter K_{ab}, defining ferromagnetic direct exchange, is small, with no clear correlation to the Cu–Cu distance, since the orientation of magnetic orbitals (Fig. 7) is not identical and their peripheral parts on bridging ligands depend on the chemical nature of the ligands. The contribution of the integral t_{ab}, which defines transitions between configurations, to the energy differs significantly among the complexes. Comparison of chloride and azide complexes, both containing the magnetic d_{xy} orbital (Fig. 7), highlights the role of delocalized orbital tails on the bridging ligand, since t_{ab} is larger in the latter case despite the greater Cu–Cu distance. The energy difference between covalent and ionic components of the valence bond, *U*, is very large (~ 2.3×10^5 cm^{-1}, ~24–25 eV), much greater than usually assumed in model Hamiltonians. It can be noted that this value is practically independent of ligand type and metal–metal distance. Such near invariance agrees better with results obtained in the simple Hubbard local repulsion model [107] than with data from more complex methods [109], in which:

$$U = J_{aa} - J_{ab}, \tag{32}$$

where J_{aa} and J_{ab} are one-center and the two-center Coulomb integral. The overall value of *J* deviates strongly from experiment and even has the wrong sign for the chloride complex. This shows that in the approximations considered, which nevertheless account for two main factors usually discussed in interpretations, the antiferromagnetic contribution is severely underestimated.

As follows from the above, calculations of diradical systems – particularly the exchange constant *J* and other important properties – within the simplest two-center model do not reproduce experimental data. On the other hand, they demonstrate the necessity of including configurations corresponding to excited states, i.e., invoking configuration interaction (CI). In

most CI methods, molecular orbitals from which determinants of excited states are constructed play a major role. Most often in CI methods applied to biradical systems, UHF orbitals obtained for the triplet state are used. Their main property is expressed by Brillouin's theorem, according to which the matrix element of the exact Hamiltonian between the ground-state determinant and the determinant obtained from it by single excitation is identically zero. Single excitations from the core to virtual orbitals are described by determinants that do not interact with any of these states. Single excitations from the core to active orbitals, or from active orbitals to virtual orbitals, lead to states that do not interact with the SCF triplet state but may interact with the singlet state, requiring careful analysis. As a result of excitation caused by charge transfer from the ligand to the metal, the resulting states do not interact with the triplet state. Their interaction with the singlet state is also extremely small. The off-diagonal elements t_{la} and t_{lb} of the Fock operator are equal to zero, and therefore the superexchange mechanisms, equations (28) and (31), do not affect the obtained results. Variational optimization of the orbitals in the SCF procedure determines the optimal delocalization between the ligand and the magnetic centers in such a way that these effects are included in the CI only through the valence orbitals.

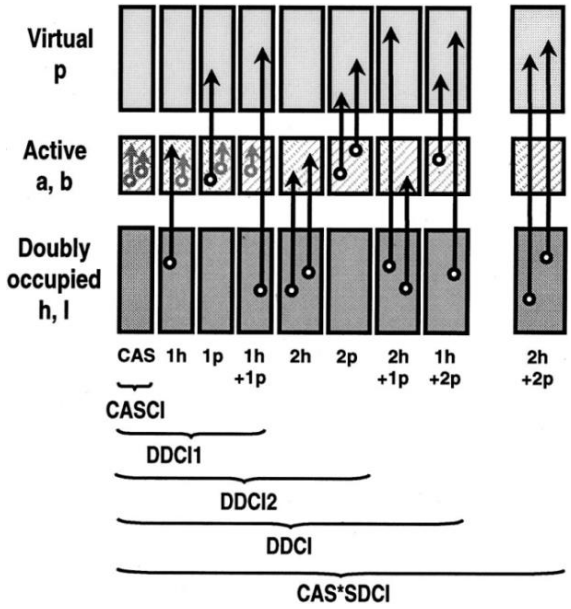

Fig. 8. Schematic representation of the various excitation operators leading to the relevant CI spaces: CAS – Complete Active Space; CASCI – Complete Active Space Configuration Interaction; DDCL1 – Difference Dedicated Configuration Interaction with taking into account single-excited configurations; DDCL2 – Difference Dedicated Configuration Interaction with taking into account single and double excited configurations; DDCI – Difference Dedicated Configuration Interaction; CAS*SDCI – Complete Active Space (CAS) reference wave function with a **S**ingles and Doubles **C**onfiguration Interaction [106]

All determinants used in constructing the CI wave function are usually denoted by numbers: n – the number of electrons excited from the core (holes) nh, and m – the number of electrons excited into the virtual space mp. Determinants employed in the quasi-degenerate perturbation theory method are designated accordingly $1h, 1p, 1h+1p, 2h$ and $2p$, as shown in Fig. 8.

When comparing results obtained by the DDCI2 and DDCI methods, it is evident that the data from DDCI are significantly closer to experimental values than those from DDCI2. It was found that the $[Cu_2Cl_6]^{2-}$ complex exhibits weak antiferromagnetism, consistent with some experimental observations [111]. Moreover, for all complexes studied, reasonable quantitative agreement with experiment was achieved. Considering the isolated contributions of the $2h + 1p$ and $1h + 2p$ determinants, several features can be noted. In particular, the overall effect of these determinants in the systems investigated is systematically antiferromagnetic. Additional calculations, in which only the $2h + 1p$ and $1h + 2p$ determinants were added to DDCI2, performed on a CuO_2 lattice fragment and on copper acetate, showed that: the contribution of the $2h + 1p$ determinant is substantial and antiferromagnetic, leading to an overestimated value of J = 1532 cm^{-1} in the cuprate and -284 cm^{-1} in acetate. The contribution of the $1h + 2p$ determinant is ferromagnetic, reducing J to -563 cm^{-1} in the cuprate and -62 cm^{-1} in acetate. The

interaction of these determinants occurs only in the fourth order of perturbation theory; therefore, the final contribution is not simply the sum of the individual effects.

The role of the polarizability of the bridging ligand is evident. The relative influence of the dispersion contribution on the overall value of J is much greater for azido- and acetate ligands, for which the magnitude of J is multiplied by a factor close to 3, compared to oxo-bridges, where the increase in J is about 30%. The case of chloride is an exception, since this effect changes the sign of the total, very small value of J.

The possibility of obtaining accurate values of the magnetic exchange constant J using *ab initio* CI calculations, particularly with the differential CI method, has been demonstrated. In such approaches, the result essentially consisted of a numerical value, without any physical analysis of the factors leading to the final J. This prevents comparison of the obtained results with qualitative models, popular among specialists in this field and often used as tools for designing new magnetic structures based on bi- and multiradical systems. An attempt to overcome this difficulty and to show that accurate calculations can be used to analyze the physical effects influencing the observed value was undertaken in [106]. Although perturbative approaches provide a natural way for such analysis, they are not quantitatively reliable, since many partial series of perturbation theory converge too slowly. A strategy was adopted based on combining localized magnetic orbitals into atom-centered magnetic orbitals and partitioning the CI space accordingly to obtain the desired information.

The most significant conclusions of [106] are as follows:

1. For physical interpretation, one cannot restrict analysis to the valence active space with a simple balance between direct exchange (K) and kinetic exchange ($-4t^2/U$), regardless of the definition of the valence space (mean-field variational or natural magnetic orbitals). The action of the exact Hamiltonian in this restricted space yields J values an order of magnitude smaller than experimental ones (and sometimes even with the wrong sign).
2. Spin polarization is not negligible, although it does not determine the main effect outside the valence space. The nature of spin polarization (ferro- or antiferro-) depends on the system.
3. The main effect beyond CAS, determined by the DDCI2 method (constructed from second-order perturbation terms), arises from external-space determinants $1h + 1p$ and represents a correction of fourth and higher orders. It consists of dynamic re-polarization of ionic structures of valence bonds.
4. Beyond the DDCI2 space, which is insufficient for quantitative agreement with experiment, excitations $2h + 1p$ and $1h + 2p$ must be considered. Their effect is substantial and does not represent dynamic ligand polarization due to charge transfer to the metal atom, but rather occurs through dynamic coupling of ligand–metal transition dipoles with transition dipoles of surrounding electrons, increasing the effective hopping integral of dispersion origin.

It is interesting and important to examine whether, and how, these various physical effects are accounted for in alternative *ab initio* methods. The NOCI method (CI using natural orbitals) certainly does not include spin-polarization effects, since it works with restricted open-shell SCF descriptions for each VB form. As it introduces only a limited number of charge-transfer states (l→a, with specific relaxations $h \rightarrow p$), chosen on fairly intuitive grounds, it clearly lacks contributions from $2h + 1p$ and $1h + 2p$ determinants, which provide opposite effects. The importance of these missing contributions may depend on the nature of the bridging ligands. The CASPT2 approach, starting from the valence CI space (minimal CAS), introduces all DDCI-type perturbations and, in principle, accounts for all of the effects discussed above. However, within this reduced scheme, the composition of the valence part of the wave functions is not revised, namely the covalent/neutral ratio in the singlet state. As shown in [58], dynamic correlation effects significantly increase this ratio (by a factor of 2–5) due to higher-order effects included in

the variational expansion. Use of reduced schemes leads to underestimation of perturbative contributions, especially when polarizable ligands are present in the molecular structure. In such cases, the remedy is to expand the CAS to include part of the higher-order effects. In [106], the above analysis was carried out using two rather different sets of orbitals: canonical Hartree–Fock orbitals and quasi-natural MOs. Magnetic orbitals are significantly more delocalized on ligands in the latter set, as observed phenomenologically [57] and justified in [106]. This effect leads to higher zero-order values of direct exchange *K* and hopping integral *t*. DDCI2 values become more accurate when natural orbitals are used, but excitations 2*h* + 1*p* and 1*h* + 2*p* still exert a significant influence on the final value of *J*. Analysis of the physical effects contributing to magnetic interactions can be quite complex. At this stage, it apparently refutes models that essentially remain confined to the valence space alone. However, as shown in [111, 112], application of effective Hamiltonian theory allows one to return to a simplified picture, i.e., to the valence model space. Use of effective energies and interactions, modified to account for complex and extensive external-space excitation effects, enables recovery of more qualitative descriptions.

NOODLEMAN'S METHOD FOR ESTIMATING THE MAGNETIC EXCHANGE CONSTANT J IN BI- AND MULTIRADICAL SYSTEMS

In [113], to examine the main features of the antiferromagnetic state of a transition-metal dimer, a single-configuration model containing nonorthogonal magnetic orbitals was proposed. A model with mixed spin symmetry and reduced spatial symmetry was developed, which has both conceptual and practical significance for computing the exchange constant *J*. To obtain the wave function of the mixed-spin state, either the unrestricted Hartree–Fock method or spin-polarized density functional theory can be employed. The most important consequence of the theory is that the Heisenberg exchange constant *J* [60] can be computed simply from the energies of the mixed-spin state and the highest pure-spin multiplet. In the proposed method, *J* is shown to be proportional to the energy difference between the state with the highest spin, $S_{\max}$, and the mixed-spin state S_0, $E(S_{\max}) - E_B$, when both energies are determined by SCF calculations. Here, E_B is the energy of the broken-symmetry state. Based on the recurrence relation for E(S) given in [113], the energies of all spin states can be obtained, allowing calculation of the difference:

$$E(S_{\max}) - E_B = \left(S_{\max}(S_{\max}+1) + \sum_{S=0}^{S_{\max}} A_1(S) \cdot S(S+1) \right) J. \tag{33}$$

For the coefficients $A_1(S)$, the following equality holds:

$$\sum_{S=0}^{S=\max} A_1(S) = 1, \tag{34}$$

which leads to:

$$\sum_{S=0}^{S_{\max}} A_1(S) \cdot S(S+1) = n = S_{\max}, \tag{35}$$

where *n* is the number of pairs of magnetic orbitals.
And that's why

$$E(S_{\max}) - E_B = -S_{\max}^2 J. \tag{36}$$

For most weakly bound dimers $|J_{AF}| \geq |J_A|$ and the antiferromagnetic terms J_{AF} dominate the contribution to *J*. From Eq. (36), it follows that the value of *J* can be computed without explicit evaluation of individual Hamiltonian matrix elements or overlap integrals S_{ab}. This is possible because the terms $E(S_{\max})$ and E_B are included through their influence on the energies of the mixed-spin and high-spin states. For comparison with Eq. (34), the energy difference between the high-spin and singlet states is:

$$E(S_{\max}) - E_0 = -S_{\max}(S_{\max}+1)J\,. \tag{37}$$

The concept described above can also be applied to calculate *J* upon addition of one electron to a molecule, forming a reduced dimer. In this situation, the added electron usually resides in a localized orbital at one end of the dimer, and the two interacting subunits become distinct; the monomers exhibit different geometries, charge distributions, and other one-electron properties. Upon addition of one electron to the oxidized dimer, reducing the number of unpaired spins on one monomer, the interacting monomers acquire spins $S_1 = n/2;\ S_2 = (n-1)/2;\ S = S_1 + S_2$. Then:

$$E(S_{\max}) - E_B = \left(-S_{\max}\left(S_{\max}+1\right) + \sum_{S=1/2}^{S_{\max}} A_1(S)\cdot S(S+1) \right) J, \tag{38}$$

where

$$A_1 = \frac{(2S+1)(n-1)!\,n!}{(n-S-1/2)!\,(n+S+1/2)!}\,. \tag{39}$$

The physical requirements for the validity of the Heisenberg Hamiltonian are stricter for the reduced dimer than for the oxidized one, so the reduced dimer can only approximately be characterized by a single value of *J*.

The most important results of [113] are contained in Eqs. (33), (36), and (38), which relate the Heisenberg exchange constant *J* to the energy difference between two independent single-configuration energy calculations $E(S_{\max})$ and E_B. These equations are equivalent to the configuration interaction approach using second-order perturbation theory with a local orbital basis [109]. The approach outlined above can be regarded as a proof of the validity of the Heisenberg Hamiltonian for two identical, weakly interacting subunits. Since the proof assumes that second-order perturbation theory provides a good approximation, and the overlap integral of the magnetic orbitals serves as the perturbation expansion parameter, it is evident that small overlaps of magnetic orbitals are required for the physical justification of using the Heisenberg Hamiltonian.

In general, for generating the wave functions and matrix elements employed in the preceding equations, either the unrestricted Hartree–Fock method or spin-polarized density functional theory can be applied. One of the advantages of broken-symmetry wave functions is that, being single-configuration wave functions, they are easily visualized.

Moreover, a broken-symmetry wave function represents a weighted average of pure spin states, which are orthogonal and do not interact with the overall Hamiltonian of the system. This is a very powerful result that can be used to evaluate the energies and properties of pure spin states.

CONCLUSIONS

The unique electronic structure of diradical and multiradical systems can be described as an open-shell singlet ground electronic state. The character of such systems is not a directly

observable property but rather represents a quantum-chemical index, originally defined as twice the weight of the double-excitation configuration in the multiconfigurational self-consistent field (MC-SCF) method. In the study of these systems, the two-electron valence configuration interaction (2e-VCI) model has proven particularly useful, allowing the identification of their nonlinear optical (NLO) properties and enabling classification according to the value of the chemical index *y*. Within the 2e-VCI framework, molecular properties (excitation energies, transition dipole moments, dipole moments, and second hyperpolarizability) for four-electron states are expressed as functions of the diradical character, which is valuable for understanding photochemical properties as well as deriving structure–property relationships in open-shell molecular systems. It has been demonstrated that the second hyperpolarizability is enhanced in the intermediate region of diradical character compared to other regimes. This principle also extends to the first hyperpolarizability β for heterosymmetric open-shell singlet systems. Such results provide the basis for introducing a new class of open-shell singlet systems that are expected to surpass traditional closed-shell NLO systems.

Based on different values of diradical character, fullerenes were divided into three distinct groups according to the parameter y_i described above. According to the obtained data, closed-shell fullerenes include C_{20}, C_{60}, and C_{70}, whereas C_{26} and C_{36}, as well as C_{30}, C_{40}, C_{42}, and C_{48}, correspond to radical and intermediate open-shell compounds, respectively.

Application of the CASPT2 method, starting from the valence CI space (minimal CAS), accounts for the effects of all DDCI perturbations. However, within this reduced scheme, the composition of the valence part of the wave functions (specifically, the covalent/neutral ratio in the singlet state) is not revised. Dynamic correlation effects significantly increase this ratio (by a factor of 2–5) due to higher-order effects included in the variational expansion. The use of reduced schemes leads to underestimation of perturbations, particularly when polarizable ligands are present in the molecular structure. In such cases, the recommended approach is to expand the CAS to incorporate part of the higher-order effects.

For approximate calculations of closed-shell systems containing two radical centers with different magnetic spin quantum numbers, Noodleman's approach has proven convenient. In this method, to describe the main features of the antiferromagnetic state of a transition-metal dimer, a single-configuration model with nonorthogonal magnetic orbitals was proposed. A model with mixed spin symmetry and reduced spatial symmetry was developed, which has both conceptual and practical significance for computing the exchange coupling constant *J*. To obtain the wave function of the mixed-spin state, either the unrestricted Hartree–Fock method or spin-polarized density functional theory can be employed. The most important consequence of this theory is that the Heisenberg exchange coupling constant *J* can be directly calculated from the energies of the mixed-spin state and the higher pure-spin multiplet.

REFERENCES

1. Salem L., Rowland C. The Electronic Properties of Diradicals. *Angew. Chem. Int. Ed. Engl.* 1972. **11**: 92.
2. Krylov A. I. Spin-Flip Configuration Interaction: An Electronic Structure Model for the Description of Excited States, Bond Breaking, and Biradicals. *Acc. Chem. Res.* 2006. **39**: 83.
3. Breher F. Single-Molecule Magnets and Related Systems. *Coord. Chem. Rev.* 2007. **251**: 1007.
4. Bradley A. Z., Kociolek M. G., Johnson R. P. Diradical Cyclizations of Enediynes. *J. Org. Chem.* 2000. **65**: 7134.
5. Quadrelli P., Romano S., Toma L., Caramella P. Cyclization Reactions of Diradicals. *Tetrahedron Lett.* 2002. **43**: 8785.
6. Gozem S., Huntress M., Schapiro I., Lindh R., Granovsky A. A., Angeli C., Olivucci M. Excited-State Dynamics of Diradicals. *J. Chem. Theory Comput.* 2012. **8**: 4069.

7. Gozem S. Schapiro I., Ferré N., Olivucci M. The molecular mechanism of thermal noise in rod photoreceptors. *Science*. 2012. **337**: 1225.
8. Wiest O., Montiel D. C., Houk K. N. Diradical Cyclizations and Electronic Properties. *J. Phys. Chem. A.* 1997. **101**: 8378.
9. Papadopoulos M. G., Sadlej A. J., Leszczynski J., Eds. *Non-linear Optical Properties of Matter – From Molecules to Condensed Phases* (Springer, Dordrecht, The Netherlands, 2006).
10. Zhou W., Kuebler S. M., Braun K. L., Yu T., Cammack J. K., Ober C. K., Perry J. W., Marder S. R. An Efficient Two-Photon-Generated Photoacid Applied to Positive-Tone 3D Microfabrication. *Science.* 2002. **296**: 1106.
11. He G. S., Tan L.-S., Zheng Q., Prasad P. N. Multiphoton Absorbing Materials: Molecular Designs, Characterizations, and Applications. *Chem. Rev*. 2008. **108**: 1245.
12. Dalton L. R., Sullivan P. A., Bale D. H. Electric Field Poled Organic Electro-Optic Materials: State of the Art and Future Prospects. *Chem. Rev*. 2010. **110**: 25.
13. Hachmann J., Dorando J. J., Avilés M., Chan G. K.-L. The Radical Character of the Acenes: A Density Matrix Renormalization. *J. Chem. Phys.* 2007. **127**: 134309.
14. Casanova D., Head-Gordon M. Restricted Active Space Spin-Flip Configuration Interaction Approach: Theory, Implementation and Examples. *Phys. Chem. Chem. Phys.* 2009. **11**: 9779.
15. Kubo T., Shimizu A., Sakamoto M., Uruichi M., Yakushi K., Nakano M., Shiomi D., Sato K., Takui T., Morita Y., et al. Synthesis, Intermolecular Interaction, and Semiconductive Behavior of a Delocalized Singlet Biradical Hydrocarbon. *Angew. Chem. Int. Ed*. 2005. **44**: 6564.
16. Tian Y.-H., Kertesz M. Is There a Lower Limit to the CC Bonding Distances in Neutral Radical π-Dimers? The Case of Phenalenyl Derivatives. *J. Am. Chem. Soc.* 2010. **132**: 10648.
17. Hayes E. F., Siu A. K. Q. Electronic Structure of the Open Forms of Three-Membered Rings. *J. Am. Chem. Soc.* 1971. **93**: 2090.
18. Yamaguchi K. In Self-Consistent Field: Theory and Applications; Carbo R., Klobukowski M., Eds.; Elsevier, Amsterdam, The Netherlands, 1990; pp 727.
19. Yamaguchi K. The Electronic Structures of Biradicals in the Unrestricted Hartree-Fock Approximation. *Chem. Phys. Lett.* 1975. **33**: 330.
20. Calzado C. J., Cabrero J., Malrieu J. P., Caballol R. Analysis of the Magnetic Coupling in Binuclear Complexes. I. Physics of the Coupling. *J. Chem. Phys.* 2002. **116**: 2728.
21. Nakano M., Kishi R., Ohta S., Takahashi H., Kubo T., Kamada K., Ohta K., Botek E., Champagne B. Relationship between Third-Order Nonlinear Optical Properties and Magnetic Interactions in Open-Shell Systems: A New Paradigm for Nonlinear Optics. *Phys. Rev. Lett.* 2007. **99**: 033001.
22. Minami T., Ito S., Nakano M. Signature of Singlet Open-Shell Character on the Optically Allowed Singlet Excitation Energy and Singlet–Triplet Energy Gap. *J. Phys. Chem. A* 2013. **117**: 2000.
23. Nakano M. Excitation Energies and Properties of Open-Shell Singlet Molecules: Applications to a New Class of Molecules for Nonlinear Optics and Singlet Fission. Springer, Heidelberg, Germany, 2014.
24. Nakano M., Kishi R., Nitta T., Kubo T., Nakasuji K., Kamada K., Ohta S., Botek E., Champagne B. Second Hyperpolarizability (γ) of Singlet Diradical Systems: Dependence of γ on the Diradical Character. *J. Phys. Chem. A* 2005. **109**: 885.
25. Nakano M., Nagao H., Yamaguchi K. Many-Electron Hyperpolarizability Density Analysis: Application to Dissociation Process of One-Dimensional H_2. *Phys. Rev. A* 1997. **55**: 1503.
26. Nakano M., Kishi R., Nakagawa N., Ohta S., Takahashi H., Furukawa S., Kamada K., Ohta K., Champagne B., Botek E., et al. Second Hyperpolarizabilities (γ) of Bisimidazole

and Bistriazole Benzenes: Diradical Character, Charged State and Spin State Dependences. *J. Phys. Chem. A* 2006. **110**: 4238.
27. Nakano M., Kubo T., Kamada K., Ohta K., Kishi R., Ohta S., Nakagawa N., Takahashi H., Furukawa S., Morita Y., et al. Second Hyperpolarizabilities of Polycyclic Aromatic Hydrocarbons Involving Phenalenyl Radical Units. *Chem. Phys. Lett.* 2006. **418**: 142.
28. Fukui H., Kishi R., Minami T., Nagai H., Takahashi H., Kubo T., Kamada K., Ohta K., Champagne B., Botek E., et al. Theoretical Study on Second Hyperpolarizabilities of Singlet Diradical Square Planar Nickel Complexes Involving o-Semiquinonato Type Ligands. *J. Phys. Chem. A* 2008. **112**: 8423.
29. Fukui H., Nakano M., Shigeta Y., Champagne B. Origin of the Enhancement of the Second Hyperpolarizabilities in Open-Shell Singlet Transition Metal Systems with Metal–Metal Multiple Bonds. *J. Phys. Chem. Lett.* 2011. **2**: 2063.
30. Okuno K., Shigeta Y., Kishi R., Nakano M. Photochromic Switching of Diradical Character: Design of Efficient Nonlinear Optical Switches. *J. Phys. Chem. Lett.* 2013. **4**: 2418.
31. Kamada K., Fuku-en S.-I., Minamide S., Ohta K., Kishi R., Nakano M., Matsuzaki M., Okamoto H., Higashikawa H., Inoue K., et al. Impact of Diradical Character on Two-Photon Absorption: Bis(acridine) Dimers Synthesized from an Allenic Precursor. *J. Am. Chem. Soc.* 2013. **135**: 232.
32. Das S., Lee S., Son M., Zhu X., Zhang W., Zheng B., Hu P., Zeng Z., Sun Z., Zeng W., et al. para-Quinodimethane-Bridged Perylene Dimers and Pericondensed Quaterrylenes: The Effect of the Fusion Mode on the Ground States and Physical Properties. *Chem.–Eur. J.* 2014. **20**: 11410.
33. Kishida H., Hibino K., Nakamura A., Kato D., Abe J. Third-Order Nonlinear Optical Properties of a π-Conjugated Biradical Molecule Investigated by Third-Harmonic Generation Spectroscopy. *Thin Solid Films.* 2010. **519**: 1028.
34. Takauji K., Suizu R., Awaga K., Kishida H., Nakamura A. Third-Order Nonlinear Optical Properties and Electroabsorption Spectra of an Organic Biradical, [Naphtho[2,1-d:6,5-d']bis([1,2,3]-dithiazole)]. *J. Phys. Chem. C* 2014. **118**: 4303.
35. Pozun Z. D., Su X., Jordan K. D. Electronic Properties of Diradical Systems. *J. Am. Chem. Soc.* 2013. **135**: 13862.
36. Abe M. Diradicals. *Chem. Rev.* 2013. **113**: 7011.
37. Douglas J. E., Rabinovitch B. S., Looney F. S. Electronic Structure of Diradicals. *J. Chem. Phys.* 1955. **23**: 315.
38. Lopez X., Piris M., Matxain J. M., Ruiperez F., Ugalde J. M. Diradical Character in Organic Molecules. *ChemPhysChem.* 2011. **12**: 1673.
39. Mahapatra U. S., Chattopadhyay S., Chaudhuri R. K. Computational Studies of Diradicals. *J. Comput. Chem.* 2011. **32**: 325.
40. Shao Y., Head-Gordon M., Krylov A. I. Electronic Structure of Diradicals by Spin-Flip Methods. *J. Chem. Phys.* 2003. **118**: 4807.
41. Schaefer H. F. III. Diradicals and Their Role in Chemistry. *Science.* 1986. **231**: 1100.
42. *International Union of Pure and Applied Chemistry (IUPAC). Biradical (B00671)* (IUPAC Gold Book, Retrieved 2024-12-12).
43. Schulz A. Group 15 Biradicals: Synthesis and Reactivity of Cyclobutane-1,3-diyl and Cyclopentane-1,3-diyl Analogues. *Dalton Trans.* 2018. **47**: 12827.
44. *International Union of Pure and Applied Chemistry (IUPAC). Diradicals (D01765)*. (IUPAC Gold Book, Retrieved 2024-12-12).
45. Bresien J., Eickhoff L., Schulz A., Zander E.; Reedijk J., Poeppelmeier K. R., Eds. Biradicals in Main Group Chemistry: Synthesis, Electronic Structure, and Application in Small-Molecule Activation. In: *Comprehensive Inorganic Chemistry III (Third Edition)*; Elsevier, Oxford, 2023; pp 165.

46. Hinz A., Bresien J., Breher F., Schulz A. Heteroatom-Based Diradical(oid)s. *Chem. Rev.* 2023. **123**: 10468.
47. Stuyver T., Chen B., Zeng T., Geerlings P., De Proft F., Hoffmann R. Do Diradicals Behave Like Radicals? *Chem. Rev.* 2019. **119**: 11291.
48. Hinz A., Kuzora R., Rosenthal U., Schulz A., Villinger A. Activation of Small Molecules by Phosphorus Biradicaloids. *Chem.–Eur. J.* 2014. **20**: 14659.
49. Kishi R., Murata Y., Saito M., Morita K., Abe M., Nakano M. Theoretical Study on Diradical Characters and Nonlinear Optical Properties of 1,3-Diradical Compounds. *J. Phys. Chem. A* 2014. **118**: 10837.
50. Hu X., Wang W., Wang D., Zheng Y. The Electronic Applications of Stable Diradicaloids: Present and Future. *J. Mater. Chem. C* 2018. **6**: 11232.
51. Bresien J., Kröger-Badge T., Lochbrunner S., Michalik D., Müller H., Schulz A., Zander E. A Chemical Reaction Controlled by Light-Activated Molecular Switches Based on Hetero-Cyclopentanediyls. *Chem. Sci.* 2019. **10**: 3486.
52. Hayes E. F., Siu A. K. Q. Electronic Structure of the Open Forms of Three-Membered Rings. *J. Am. Chem. Soc.* 1971. **93**: 2090.
53. Herebian D., Wieghardt K. E., Neese F. Analysis and Interpretation of Metal-Radical Coupling in a Series of Square Planar Nickel Complexes: Correlated Ab Initio and Density Functional Investigation of $[Ni(LISQ)_2]$. *J. Am. Chem. Soc.* 2003. **125**: 10997.
54. Bachler V., Olbrich G., Neese F., Wieghardt K. Theoretical Evidence for the Singlet Diradical Character of Square Planar Nickel Complexes Containing Two o-Semiquinonato Type Ligands. *Inorg. Chem.* 2002. **41**: 4179.
55. Jung Y., Head-Gordon M. How Diradicaloid Is a Stable Diradical? *ChemPhysChem.* 2003. **4**: 522.
56. Doehnert D., Koutecky J. Occupation Numbers of Natural Orbitals as a Criterion for Biradical Character. Different Kinds of Biradicals. *J. Am. Chem. Soc.* 1980. **102**: 1789.
57. Lineberger W. C., Borden W. T. The Synergy between Qualitative Theory, Quantitative Calculations, and Direct Experiments in Understanding, Calculating, and Measuring the Energy Differences between the Lowest Singlet and Triplet States of Organic Diradicals. *Phys. Chem. Chem. Phys.* 2011. **13**: 11792.
58. Nguyen K. A., Gordon M. S., Boatz J. A. The Inversion of Bicyclobutane and Bicyclodiazoxane. *J. Am. Chem. Soc.* 1994. **116**: 9241.
59. Jain R., Snyder G. J., Dougherty D. A. Direct ESR Observation of the Localized Biradical 1,3-Dimethyl-1,3-Cyclobutadiyl. *J. Am. Chem. Soc.* 1984. **106**: 7294.
60. Heisenberg W. Zur Theorie des Ferromagnetismus. *Eur. Phys. J. A.* 1928. **49**: 619.
61. Nakano M., Kishi R., Ohta S., Takebe A., Takahashi H., Furukawa S., Kubo T., Morita Y., Nakasuji K., Yamaguchi K., et al. Origin of the Enhancement of the Second Hyperpolarizability of Singlet Diradical Systems with Intermediate Diradical Character. *J. Chem. Phys.* 2006. **125**: 074113.
62. Nakano M., Champagne B. Diradical Character Dependences of the First and Second Hyperpolarizabilities of Asymmetric Open-Shell Singlet Systems. *J. Chem. Phys.* 2013. **138**: 244306.
63. Nakano M., Champagne B. Theoretical Design of Open-Shell Singlet Molecular Systems for Nonlinear Optics. *J. Phys. Chem. Lett.* 2015. **6**: 3236.
64. Castet F., Rodriguez V., Pozzo J. L., Ducasse L., Plaquet A., Champagne B. Design and Characterization of Molecular Nonlinear Optical Switches. *Acc. Chem. Res.* 2013. **46**: 2656.
65. Ohta S., Nakano M., Kubo T., Kamada K., Ohta K., Kishi R., Nakagawa N., Champagne B., Botek E., Takebe A., et al. Theoretical Study on the Second Hyperpolarizabilities of Phenalenyl Radical Systems Involving Acetylene and Vinylene Linkers: Diradical Character and Spin Multiplicity Dependences. *J. Phys. Chem. A* 2007. **111**: 3633.

66. Nakano M., Minami T., Yoneda K., Muhammad S., Kishi R., Shigeta Y., Kubo T., Rougier L., Champagne B., Kamada K., et al. Giant Enhancement of the Second Hyperpolarizabilities of Open-Shell Singlet Polyaromatic Diphenalenyl Diradicaloids by an External Electric Field and Donor–Acceptor Substitution. *J. Phys. Chem. Lett.* 2011. **2**: 1094.
67. Matsui H., Fukuda K., Takamuku S., Sekiguchi A., Nakano M. Theoretical Study on the Relationship between Diradical Character and Second Hyperpolarizabilities of Four-Membered-Ring Diradicals Involving Heavy Main Group Elements. *Chem.–Eur. J.* 2015. **21**: 2157.
68. Fukuda K., Nozawa T., Yotsuyanagi H., Ichinohe M., Sekiguchi A., Nakano M. Theoretical Study on the Enhancement of the Second Hyperpolarizabilities of Si-, Ge-Disubstituted Quinodimethanes: Synergy Effects of Open-Shell Nature and Intramolecular Charge Transfer. *J. Phys. Chem. C* 2015. **119**: 1188.
69. Yoneda K., Nakano M., Fukuda K., Matsui H., Takamuku S., Hirosaki Y., Kubo T., Kamada K., Champagne B. Third-Order Nonlinear Optical Properties of One-Dimensional Open-Shell Molecular Aggregates Composed of Phenalenyl Radicals. *Chem.–Eur. J.* 2014. **20**: 11129.
70. Fukui H., Takamuku S., Yamada T., Fukuda K., Takebayashi T., Shigeta Y., Kishi R., Champagne B., Nakano M. Open-Shell Character and Second Hyperpolarizabilities of One-Dimensional Chromium(II) Chains: Size Dependence and Bond-Length Alternation Effect. *Inorg. Chem.* 2014. **53**: 8700.
71. Son Y.-W., Cohen M. L., Louie S. G. Half-Metallic Graphene Nanoribbons. *Nature.* 2006. **444**: 347.
72. Muhammad S., Fukuda K., Minami T., Kishi R., Shigeta Y., Nakano M. Interplay between the Diradical Character and Third-Order Nonlinear Optical Properties in Fullerene Systems. *Chem.–Eur. J.* 2013. **19**: 1677.
73. Bonness S., Fukui H., Yoneda K., Kishi R., Champagne B., Botek E., Nakano M. Third-Order Nonlinear Optical Properties of Diradical Systems. *Chem. Phys. Lett.* 2010. **493**: 195.
74. Nakano M., Kishi R., Yoneda K., Inoue Y., Inui T., Shigeta Y., Kubo T., Champagne B. Diradical Character and Nonlinear Optical Properties. *J. Phys. Chem. A* 2011. **115**: 8767.
75. Yamaguchi K. In Self-Consistent Field: Theory, Applications; Carbo R., Klobukowski M., Eds.; Elsevier, Amsterdam, 1990; p. 727.
76. Nakano M., Fukui H., Minami T., Yoneda K., Shigeta Y., Kishi R., Champagne B., Botek E., Kubo T., Ohta K., Kamada K. Diradical Character and Nonlinear Optical Properties of Open-Shell Systems. *Theor. Chem. Acc.* 2011. **130**: 711.
77. Nakano M., Minami T., Fukui H., Yoneda K., Shigeta Y., Kishi R., Champagne B., Botek E. Diradical Character and Nonlinear Optical Properties. *Chem. Phys. Lett.* 2010. **501**: 140.
78. Nakano M., Kishi R., Ohta S., Takebe A., Takahashi H., Furukawa S., Takashi K., Morita Y., Nakasuji K., Yamaguchi K., Kamada K., Ohta K., Champagne B., Botek E. Origin of the Enhancement of the Second Hyperpolarizability of Singlet Diradical Systems with Intermediate Diradical Character. *J. Chem. Phys.* 2006. **125**: 074113.
79. Hayes E. F., Siu A. K. Q. Electronic Structure of the Open Forms of Three-Membered Rings. *J. Am. Chem. Soc.* 1971. **93**: 2090.
80. Takatsuka K., Fueno T., Yamaguchi K. Theoretical Studies on Diradical Systems. *Theor. Chim. Acta* 1978. **48**: 175.
81. Head-Gordon M. Electronic Structure of Diradicals by Spin-Flip Methods. *Chem. Phys. Lett.* 2003. **372**: 508.
82. Clar E. *Polycyclic Hydrocarbons* (Academic Press, New York, 1964).

83. Nakano M., Kishi R., Ohta S., Takahashi H., Kubo T., Kamada K., Ohta K., Botek E., Champagne B. Relationship between Third-Order Nonlinear Optical Properties and Magnetic Interactions in Open-Shell Systems. *Phys. Rev. Lett.* 2007. **99**: 033001.
84. Ohta S., Nakano M., Kubo T., Kamada K., Ohta K., Kishi R., Nakagawa N., Champagne B., Botek E., Takebe A., Umezaki S., Nate M., Takahashi H., Furukawa S., Morita Y., Nakasuji K., Yamaguchi K. Electronic Structure of Open-Shell Singlet Molecules: Diradical Character and Third-Order Nonlinear Optical Properties. *J. Phys. Chem. A.* 2007. **111**: 3633.
85. Yoneda K., Nakano M., Fukui H., Minami T., Shigeta Y., Kubo T., Botek E., Champagne B. Open-Shell Characters and Second Hyperpolarizabilities of One-Dimensional Graphene Nanoflakes Composed of Trigonal Graphene Units. *ChemPhysChem.* 2011. **12**: 1697.
86. Verdaguer M., Bleuzen A., Marvaud V., et al. Molecular Magnets: Prussian Blue Analogues and Related Systems. *Coord. Chem. Rev.* 1999. **190–192**: 1023.
87. Kahn O. *Molecular Magnetism* (VCH: New York, 1993).
88. Van Vleck J. H. *The Theory of Electric and Magnetic Susceptibilities* (Oxford University Press: Oxford, 1932).
89. Fabrizi de Biani F., Ruiz E., Cano J., Novoa J. J., Alvarez S. Magnetic Coupling in End-to-End Azido-Bridged Copper and Nickel Binuclear Complexes: A Theoretical Study. *Inorg. Chem.* 2000. **39**: 3221.
90. Adamo C., Barone V., Bencini A., Totti F., Ciofini I. Modeling Magnetic Exchange Interactions in Weakly Bonded Systems: Broken Symmetry Approach and Density Functional Calculations. *Inorg. Chem.* 1999. **38**: 1996.
91. Caro J., Alemany P., Alvarez S., Verdaguer M., Ruiz E. Exchange Coupling in Oxalato-Bridged Copper(II) Binuclear Compounds: A Density Functional Study. *Chem.–Eur. J.* 1998. **4**: 476.
92. Noodleman L., Norman J. G., Jr. The Electronic Structure of Metal–Metal Bonds: Broken Symmetry Approach. *J. Chem. Phys.* 1979. **70**: 4903.
93. Broer R., Nieuwpoort W. C. Broken Orbital Symmetry and the Description of Valence Hole States in the Tetrahedral $[CrO_4]^{2-}$ Anion. *Theor. Chim. Acta*. 1998. **73**: 405.
94. van Oosten A. B., Broer R., Nieuwpoort W. C. Heisenberg Exchange Enhancement by Orbital Relaxation in Cuprate Compounds. *Chem. Phys. Lett.* 1996. **257**: 207.
95. van Oosten A. B., Broer R., Nieuwpoort W. C. Heisenberg Exchange in La_2CuO_2. *Int. J. Quantum Chem., Quantum Chem. Symp.* 1995. **29**: 241.
96. de Graaf C., Broer R., Nieuwpoort W. C. Magnetic Coupling in Transition Metal Complexes. *Chem. Phys. Lett.* 1997. **271**: 372.
97. de Graaf C., de P. R. Moreira I., Illas F. Electronic Structure of Binuclear Complexes. *Int. J. Mol. Sci.* 2000. **1**: 28.
98. de Graaf C., Sousa C., de P. R. Moreira I., Illas F. Magnetic Properties of Transition Metal Complexes. *J. Phys. Chem. A* 2001. **105**: 11371.
99. Miralles J., Castell O., Caballol R., Malrieu J. P. Configuration Interaction Studies of Magnetic Coupling. *Chem. Phys.* 1993. **172**: 33.
100. Castell O., Caballol R. Electronic Structure of Inorganic Complexes. *Inorg. Chem.* 1999. **38**: 668.
101. Cabrero J., Ben Amor N., de Graaf C., Illas F., Caballol R. Magnetic Coupling in Organic and Inorganic Systems. *J. Phys. Chem. A* 2000. **104**: 9983.
102. Calzado C. J., Sanz J. F., Malrieu J. P. Analysis of Magnetic Coupling in Binuclear Complexes. *J. Chem. Phys.* 2000. **112**: 5158.
103. Calzado C. J., Malrieu J. P. Magnetic Coupling in Extended Systems. *Phys. Rev. B* 2001. **63**: 214520.

104. Miralles J., Daudey J. P., Caballol R. Configuration Interaction and Magnetic Coupling. *Chem. Phys. Lett.* 1992. **198**: 555.
105. de Loth P., Cassoux P., Daudey J. P., Malrieu J. P. Magnetic Coupling in Binuclear Complexes. *J. Am. Chem. Soc.* 1981. **103**: 4007.
106. Calzado C. J., Cabrero J., Malrieu J. P., Caballol R. Analysis of the Magnetic Coupling in Binuclear Complexes. I. Physics of the Coupling. *J. Chem. Phys.* 2002. **116**: 2728.
107. Anderson P. W. *In Theory of the Magnetic Interaction: Exchange in Insulators and Superconductors* (Academic Press, New York, 1963).
108. Kahn O., Briat B. Magnetic Exchange in Transition Metal Complexes. *J. Chem. Soc., Faraday Trans. 2* 1976. **72**: 268.
109. Hay P. J., Thibeault J. C., Hoffmann R. Orbital Interactions in Metal Complexes. *J. Am. Chem. Soc.* 1975. **97**: 488.
110. Geertsma W. Electronic Structure and Magnetic Properties of Transition Metal Compounds. *Physica B* 1990. **164**: 241.
111. Calzado C. J., Angeli C., Caballol R., Malrieu J.-P. Analysis of the Magnetic Coupling in Binuclear Systems. III. The Role of the Ligand-to-Metal Charge Transfer Excitations Revisited. *Chem. Phys.* 2009. **131**: 044327.
112. Cabrero J., Calzado C. J., Maynau D., Caballol R., Malrieu J. P. Metal–Ligand Delocalization in Magnetic Orbitals of Binuclear Complexes. *J. Phys. Chem. A* 2002. **106**: 8870.
113. Noodleman L. Valence Bond Description of Antiferromagnetic Coupling in Transition Metal Dimers. *J. Chem. Phys.* 1981. **74**: 5737.

УДК 544.18 *DOI: 10.15407/Surface.2025.17.118*

ДИРАДИКАЛЬНІ ТА МУЛЬТИРАДИКАЛЬНІ СИСТЕМИ ТА КВАНТОВОХІМІЧНІ МЕТОДИ ОБЧИСЛЕННЯ ЇХНІХ ВЛАСТИВОСТЕЙ

О. С. Кремень, В. В. Лобанов

Інститут хімії поверхні ім. О. О. Чуйка НАН України,
вул. Олега Мудрака, 17, Київ, 03164, Україна, е-пошта: kremenoksana@ukr.net

Підвищений інтерес до дирадикальних сполук (ди- та мульти-) зумовлений їхніми унікальними нелінійними оптичними властивостями (NLO), що проявляються як відгук на дію сильних електричних полів лазерів. Їхні NLO знаходять численні застосування у спектроскопії, матеріалознавстві та інженерії, а також у зборі, зберіганні, обробці й передачі даних за допомогою фотонів. Електронна структура дирадикальних систем з відкритою оболонкою класифікується за величиною їхнього дирадикального характеру (y) відповідно до трьох категорій: (i) системи із замкненою оболонкою (y = 0); (ii) проміжні дирадикальні системи (0 < y < 1); (iii) системи з чистою відкритою оболонкою (y = 1). Через взаємодію між неспареними електронами у дирадикальних частинках їх не можна просто розглядати як спільну систему двох незалежних радикальних центрів. Для повного опису електронної структури дирадикальних частинок необхідно враховувати як відкриті оболонки синглетних, так і триплетних станів. Результати, отримані в рамках простої двоцентрової моделі, приводять до появи нового класу систем з відкритою оболонкою у синглетному стані, які, як очікується, перевищать традиційні NLO-системи із замкненою оболонкою. На основі цього принципу запропоновано практичні рекомендації

щодо молекулярного дизайну та оптимізації дирадикальних характеристик і, відповідно, для посилення NLO на основі даних розрахунків із перших принципів, виконаних на реалістичних молекулярних системах з відкритою оболонкою у синглетному стані. Отримані розрахункові дані щодо фулеренів корисні не лише для розробки ефективних NLO-матеріалів на їхній основі, але й для розуміння походження мультирадикального характеру деяких зв'язків у таких системах. Хоча досліджені фулеренові структури мають синглетні основні електронні стани, їхній проміжний дирадикальний характер може призводити до звуження енергетичного зазору між синглетними станами та станами з більш високими мультиплетами. При розгляді молекулярного магнетизму показано, що основний ефект поза межами CAS, визначений методом DDCI2 (побудованим із членів другого порядку теорії збурень), зумовлений детермінантами зовнішнього простору типу 1h + 1p і є поправкою четвертого та вищих порядків. Він полягає у динамічній повторній поляризації іонних структур валентних зв'язків. При виході за межі простору DDCI2, який не забезпечує досягнення кількісної узгодженості з експериментом, необхідно враховувати збудження типу 2h + 1p та 1h + 2p. Їхній ефект є досить суттєвим і не становить динамічної поляризації ліганда через перенесення заряду на атом металу, а відбувається через динамічне спряження диполів переходів ліганд–метал із диполями переходів навколишніх електронів та збільшення ефективного інтеграла перескоку дисперсійного походження. У рамках методу Нудлемана показано, що для генерації хвильових функцій і матричних елементів, які використовуються при обчисленні енергії вищих мультиплетів, можна застосовувати як необмежений метод Хартрі–Фока, так і теорію функціонала густини зі спіновою поляризацією. Однією з переваг хвильових функцій із порушеною симетрією є те, що, будучи хвильовими функціями однієї конфігурації, вони легко візуалізуються. Крім того, хвильова функція з порушеною симетрією дає зважене середнє значення чистих спінових станів, які є ортогональними та не взаємодіють із загальним гамільтоніаном системи. Це надзвичайно потужний результат, який можна використати для оцінки енергій і властивостей чистих спінових станів.

Ключові слова: *дирадикальний стан, дирадикальний характер, синглетні стани з відкритою оболонкою, нелінійні оптичні властивості, дирадикальні стани фулеренів, числа заповнення натуральних орбіталей, константа магнітної взаємодії.*